THE JOURNAL OF BIOLOGICAL CHEMISTRY VOL. 289, NO. 18, pp. 12404–12420, May 2, 2014

A Histidine-rich Linker Region in Peptidylglycine α-Amidating Monooxygenase Has the Properties of a pH Sensor*

Received for publication, December 26, 2013, and in revised form, March 12, 2014 Published, JBC Papers in Press, March 13, 2014, DOI 10.1074/jbc.M113.545947

Kurutihalli Vishwanatha[‡], Nils Bäck[§], Richard E. Mains[‡], and Betty A. Eipper[‡¶1]

From the Departments of [‡]Neuroscience and [¶]Molecular Biology and Biophysics, University of Connecticut Health Center, Farmington, Connecticut 06030 and the [§]Institute of Biomedicine/Anatomy, University of Helsinki, FIN-00014, Helsinki, Finland

Background: Secretory granule membrane proteins are retrieved and reused or degraded after exocytosis.
Results: A pH-sensitive His cluster in the amidating enzyme is essential for its trafficking.
Conclusion: Lacking this conserved His cluster, proteolytic maturation and generation of a soluble cytosolic fragment of amidating enzyme fail to occur, disrupting secretion and nuclear signaling.
Significance: The storage and regulated secretion of peptides requires intraluminal signaling.

Decreasing luminal pH is thought to play a role in the entry of newly synthesized and endocytosed membrane proteins into secretory granules. The two catalytic domains of peptidylglycine α-amidating monooxygenase (PAM), a type I integral membrane protein, catalyze the sequential reactions that convert peptidyl-Gly substrates into amidated products. We explored the hypothesis that a conserved His-rich cluster (His-Gly-His-His) in the linker region connecting its two catalytic domains senses pH and affects PAM trafficking by mutating these His residues to Ala (Ala-Gly-Ala-Ala; H3A). Purified recombinant wild-type and H3A linker peptides were examined using circular dichroism and tryptophan fluorescence; mutation of the His cluster largely eliminated its pH sensitivity. An enzymatically active PAM protein with the same mutations (PAM-1/H3A) was expressed in HEK293 cells and AtT-20 corticotrope tumor cells. Metabolic labeling followed by immunoprecipitation revealed more rapid loss of newly synthesized PAM-1/H3A than PAM-1; although release of newly synthesized monofunctional PHM/H3A was increased, release of soluble bifunctional PAM/H3A, a product of the endocytic pathway, was decreased. Surface biotinylation revealed rapid loss of PAM-1/H3A, with no detectable return of the mutant protein to secretory granules. Consistent with its altered endocytic trafficking, little PAM-1/H3A was subjected to regulated intramembrane proteolysis followed by release of a small nuclear-targeted cytosolic fragment. AtT-20 cells expressing PAM-1/H3A adopted the morphology of wild-type AtT-20 cells; secretory products no longer accumulated in the *trans*-Golgi network and secretory granule exocytosis was more responsive to secretagogue.

Proteins destined for the secretory pathway are synthesized in the endoplasmic reticulum and traverse multiple compartments of varying pH as they travel to their final destinations. In neurons and endocrine cells that store peptides for regulated secretion, soluble cargo, and essential membrane proteins must be targeted to secretory granules. The post-translational modifications and sorting of prohormones are initiated in the dilated extensions of the *trans*-Golgi network (TGN)[2] and continue as immature secretory granules are converted into mature secretory granules and transported to their sites of release (1, 2). Intraluminal pH, which becomes increasingly acidic as proteins move from the Golgi (pH 6.7) into mature secretory granules (pH 5.2), is a key factor governing interactions among soluble cargo and granule membrane proteins and lipids (3–7).

The soluble content of the secretory granules, which includes peptide precursors, prohormone convertases, various metals, and chromogranins, are sorted and handled differently from granule membrane proteins. More than half of the peptide products require an essential α-amidation reaction at their C terminus to make them biologically active. This reaction is catalyzed only by peptidylglycine α-amidating monooxygenase (PAM), a bifunctional type I membrane protein (Fig. 1*A*) (8, 9). PAM catalyzes the α-hydroxylation of Gly-extended peptides through its hydroxylation domain (PHM) and subsequently catalyzes α-amidation through its lyase domain (PAL). PHM, PAL, and intact PAM have acidic pH optima, as do other enzymes that function in the lumen of the secretory granule (7, 10–13). The major splice variant, PAM-1, is subject to cleavage by prohormone convertases, generating soluble PHM (sPHM) and membrane PAL (Fig. 1*A*). Following granule exocytosis, PAM-1 that is deposited on the cell surface is retrieved by endocytosis and either recycled or degraded (14–16). During its endocytic trafficking, the luminal domain of PAM is again exposed to environments of descending pH. Endocytosed PAM-1 is subject to luminal cleavages that generate soluble

* This work was supported, in whole or in part, by National Institutes of Health Grant DK-32949, the Janice and Rodney Reynolds Endowment, Scoville Endowment, Liv och Hälsa Foundation, Magnus Ehrnrooth Foundation, and the Perklén Foundation.
[1] To whom correspondence should be addressed: 263 Farmington Ave., Farmington, CT 06030. Tel.: 860-679-8898; Fax: 860-679-1885; E-mail: eipper@uchc.edu.

[2] The abbreviations used are: TGN, *trans*-Golgi network; PAM, peptidylglycine α-amidating monooxygenase; PHM, peptidylglycine α-hydroxylating monooxygenase; PAL, peptidyl-α-hydroxyglycine α-amidating lyase; CSFM, complete serum-free medium; sPAM, soluble PAM; sPAL, soluble PAL; POMC, proopiomelanocortin; PHMcc, catalytic core of PHM; sf-CD, soluble fragment of the PAM cytosolic domain; TES, 2-{[2-hydroxy-1,1-bis(hydroxymethyl)ethyl]amino}ethanesulfonic acid.

PAM (sPAM) and intramembrane proteolysis that generates a soluble, cytosolic fragment of PAM (sf-CD) (Fig. 1*A*).

The acidification of both secretory granules and endosomes is accomplished by the vacuolar (H^+)-ATPase (V-ATPase), which translocates protons across TGN and endosomal membranes, thus regulating biosynthetic and endocytic trafficking in a pH-dependent manner (17–19). Several mammalian transmembrane proteins have been shown to act as pH sensing proteins; for all, the mechanism with which they sense luminal pH involves His residues (20–24). The imidazole side chain of His, with a pK_a of 6.0, is an ideal candidate to exhibit dual conformational states upon protonation/deprotonation events in the exocytic and endocytic pathways.

Receptor-mediated internalization of ligands, metals, and viral particles generally depends upon the low pH environment in the early/late endosomes for cargo release (25). A conformational change in the vesicular-stomatitis virus due to His protonation brings about membrane fusion (26, 27). A crucial role of His residues in the function of the hydrogen ion channel of the M2-protein of the influenza A virus has been demonstrated (28). A pH-dependent conformational change in two critical His residues dictates substrate binding capacity for the SARS (severe acute respiratory syndrome) coronavirus proteinase (29). At low pH, the Hisactophilins of *Dictyostelium discoideum* bind more tightly to actin and lipids; this pH-dependent response is due to a conformational change in the 31–35 His residues clustered in loops on the protein surface (30). OGR1 (ovarian cancer G protein-coupled receptor 1) was proposed to function as a proton-sensing receptor involved in blood pH homoeostasis; four His residues located on its extracellular surface play an essential role in its ability to respond to pH (20).

PHM and PAL are separated by a non-catalytic linker region (Fig. 1*A*). The linker region in PAM-2 includes only 36 amino acids, whereas the linker region in PAM-1 includes an additional 105-amino acid segment encoded by exon 16 (Fig. 1). In addition to providing a site for controlled endoproteolytic cleavage of PAM-1, exon 16 is subjected to *O*-glycosylation and this region plays an important role in the sorting, trafficking, and turnover of PAM (16). CLUSTALW analysis of evolutionarily divergent PAM proteins (31) identified a conserved His cluster in bifunctional PAM proteins from mammals and mollusks; no His cluster was found in *Danio rerio*, *Acropora*, *Schistosoma*, or *Chlamydomonas* PAM or in monofunctional *Drosophila* PHM (Fig. 1*B*). We used biophysical and cell biological approaches to test the hypothesis that this His cluster plays an essential role in the ability of PAM to serve as a pH sensor in the regulated secretory pathway.

MATERIALS AND METHODS

Protein Production and Purification—Sequences encoding exon 16 (rPAM-1(393–497)), exon 15/16 (rPAM-1(369–497)), and exon 13/15/16 (rPAM-1(357–497)) were cloned into the pGEX-6P-1 vector in reading frame with GST and expressed in BL21 *Eschrichia coli* cells; constructs were verified by DNA sequencing. Bacterial lysates (500 ml of culture) were prepared by sonication in PBS; following centrifugation, each supernatant was applied to a 5-ml GSTrap^{TM} cartridge (GE Healthcare). After washing with PBS, on-column cleavage of the fusion protein was accomplished by overnight incubation at 4 °C with HRV3C protease (80 units/500 ml of culture) (Eton Biosciences, San Diego, CA); the cartridge was washed with 20 mM NaTES (pH 7.0) to retrieve the recombinant protein. Further purification was accomplished by binding the eluate to a Q-Sepharose column equilibrated with 20 mM NaTES (pH 7.0) followed by elution with a gradient to 0.5 M NaCl in the same buffer over 60 min. Protein purity as judged by SDS-PAGE and staining with Coomassie Brilliant Blue R-250 was at least 97%; recovery was ~60–70% (5–6 mg of purified recombinant protein/500 ml of culture).

Fluorescence Spectroscopy—All fluorescence measurements were performed using a F2500 spectrofluorimeter (Hitachi, Japan) with a thermostated cell holder and a 1-cm path length quartz cuvette. Slit widths with a nominal bandpass of 10 nm were used for both excitation and emission beams. Intrinsic fluorescence emission spectra were recorded from 300 to 400 nm after excitation at 295 nm; 20 mM NaMES buffer was used for the pH 5.0 to 6.0 range and 20 mM NaTES for the pH 6.5 to 8.0 range.

Circular Dichroism—Spectra were recorded at 20 °C using a Jasco J-715 spectropolarimeter (Jasco, Easton, MD) calibrated with *d*-(+)-10-camphor sulfonic acid ammonium salt. Far UV CD spectra were recorded between 190 and 270 nm using a 1-mm path length cell and a protein concentration of 6 μM in buffers of pH 5.0–8.0. Scans were recorded three times and averaged.

In Vitro Aggregation Assay—Recombinant proteins were concentrated using Centricon concentrators with a 10-kDa cut-off membrane (Amicon). Just before use, protein stocks were pre-spun for 30 min at 22,000 × *g*; any pelleted material was discarded. A procedure similar to that previously described was employed (1). Briefly, a 50-μl sample of 0.2–0.5 mg/ml of recombinant protein in 5 mM HEPES, 10 mM MES (pH 7.5) was titrated to pH 5.5 by adding a pre-determined amount of 0.125 N HCl. After incubation at 37 °C for 1 h, samples were centrifuged at 50,000 × *g* for 20 min in a TL100 ultracentrifuge to separate aggregates from soluble protein. The supernatants were removed and aliquots of the supernatants and the entire solubilized pellets were subjected to SDS-PAGE. The gels were stained with Coomassie Brilliant Blue R-250 and band intensities were quantified using GeneTools software (Syngene).

Generation of Stable Cell Lines—Starting with the pCI-Neo-Kr PAM-1 vector, the Stratagene QuikChange protocol (La Jolla, CA) was used to replace His^{364}, His^{366}, and His^{367} with Ala; the DNA sequence of the pCI-Neo-Kr PAM-1/H3A vector was verified. AtT-20 cells were grown in Dulbecco's modified Eagle's medium/F-12 with 25 mM HEPES, 10% NuSerum, 10% fetal bovine serum and antibiotics (pH 7.4). To establish stable AtT-20 cell lines expressing PAM-1/H3A, 70–75% confluent cells in a T75 flask were transfected with 30 μg of pCI-Neo-Kr PAM-1/H3A vector using Lipofectamine. After drug selection (0.5 mg/ml G-418) for 3 weeks, cells were subcloned by limiting dilution. Drug-resistant lines were selected based on their ability to secrete active PHM and were again subcloned by limiting dilution. Two stable clonal cell lines were chosen for further analysis.

Secretion of PAM Activity—To assess basal secretion, AtT-20 cells in 6-well plates were incubated in complete serum-free medium (CSFM) with 0.05 mg/ml of bovine serum albumin (3 ml/well) for 24 h; spent medium was centrifuged to remove non-adherent cells and assayed for PHM activity. To measure secretagogue stimulation, cells were first rinsed with pre-warmed CSFM, and then incubated in 2 ml of CSFM for two sequential 1-h basal secretion periods. Cells were then incubated in CSFM containing no secretogogue (basal), 2 mM $BaCl_2$, or 1 μM phorbol myristate acetate for 1 h; media were collected as before and cells were extracted into 20 mM NaTES, 10 mM mannitol, 1% Triton X-100 (pH 7.4 (TMT)) for measurement of enzyme activity (32). PAM activity was quantified using [^{125}I]-Acetyl-Tyr-Val-Gly; samples were assayed in duplicate after addition of optimal amounts of exogenous copper and ascorbate (32–34). For determining the optimum pH for maximum activity, the following buffers were mixed at 50 mM each and brought to the appropriate pH using either hydrochloric acid (pH 3.0) or sodium hydroxide (pH 3.5–8.0): homo-PIPES, MES, and HEPES.

Intracellular pH gradients were collapsed by treating PAM-1 and PAM-1/H3A AtT-20 cells with alkalinizing drugs in complete serum-free medium for 24 h. Ammonium chloride and methylamine (Sigma) were used at 2.5 and 5 mM, respectively. Concanamycin A (Sigma) in dimethyl sulfoxide was used at 1 nM to block the vacuolar H^+-ATPase (V-ATPase); alkalinization was assessed in living drug-treated cells using acridine orange (35). After drug treatment, media were collected and cells were extracted into TMT as described above.

Immunofluorescence—Cells grown on glass chamber slides were rinsed with PBS (50 mM sodium phosphate, 150 mM NaCl, pH 7.4) and fixed in 4% paraformaldehyde in PBS for 20 min at room temperature. Cells were then sequentially incubated in PBS containing 0.075% Triton X-100 for 20 min at RT, PBS containing BSA (2 mg/ml) for 1 h, and PBS containing BSA and primary antibodies (diluted 1:1000) for 2 h. The primary antibodies used were: γMSH (JH189 (9)), C terminus of ACTH(1–39) (JH44 (36)), GM130 (Golgi marker; BD Biosciences), PHM (JH1761 (8)), PAL (JH256 (38)), PAM-CD (C-STOP, CT267 (39)), and exon 16 (JH629 (40)). Primary antibodies were visualized using Cy3-conjugated donkey anti-mouse IgG (code 715-166-151; Jackson ImmunoResearch) and fluorescein isothiocyanate-conjugated goat anti-rabbit IgG (code 711-096-152, Jackson ImmunoResearch). Slides were mounted with glass coverslips using ProLong Gold antifade mounting agent (Invitrogen).

Cell Dimension Measurements—Phase-contrast images were taken under identical conditions using a ×20 objective and a Nikon TE300 microscope. Five individual images for each cell type (total 50 cells) were analyzed for total cell area, length, and breadth using image analysis software (NIS elements).

Electron Microscopy—For transmission electron microscopy cells were fixed with 2.5% glutaraladehyde in 0.1 M cacodylate buffer, post-fixed with 1% osmium tetroxide and 1.5% potassium ferrocyanide, dehydrated, and embedded in an Epon resin. Ultrathin sections were post-stained with uranyl acetate and lead citrate and 30 Golgi complexes in each specimen were systematically sampled and photographed at ×6000 with a Jeol JEM-1400 electron microscope equipped with a Gatan Orius SC 1000B bottom mounted CCD camera.

For colloidal gold labeling at the electron microscope level, cells were incubated with antibody JH629 1:250 in DMEM/HEPES/BSA for 30 min at 4 °C, rinsed with DMEM/HEPES/BSA at 4 °C, incubated in DMEM/HEPES with protein A/15 nm colloidal gold (University of Utrecht, Utrecht, Netherlands) at the concentration suggested by the provider (1:60–75) for 30 min at 4 °C, rinsed in DMEM/HEPES at 4 °C, and then chased in culture medium at 37 °C. After the chase, cells were fixed with 2.5% glutaraldehyde in 0.1 M sodium cacodylate buffer and osmicated, dehydrated, and embedded in Epon as above. For classification of gold particles in multivesicular bodies, sections were systematically scanned to give 73 multivesicular bodies from two experiments in each cell line. Gold particles within 20 nm of the membrane of the multivesicular body were classified as external.

Immunoelectron Microscopy—Cells were fixed with 4% paraformaldehyde and 2% sucrose in 0.1 M phosphate buffer at room temperature, scraped, pelleted, and embedded in gelatin. Polyvinylpyrrolidone/sucrose-infiltrated specimens were sectioned at −120 °C; sections were collected with methyl cellulose/sucrose, blocked with 1% fish skin gelatin (Sigma) and 1% BSA (Sigma), and incubated with antibody JH629 (1:2000) for 1 h followed by protein A/10 nm gold (University of Utrecht) for 1 h and embedded in uranyl acetate/methylcellulose. For double staining with the ACTH C-terminal antibody, internalized PAM antibody was first detected with protein A/10 nm gold; the sections were then fixed for 5 min with 1% glutaraldehyde to block background binding and then incubated with C-terminal ACTH antibody Kathy at 1:1000 (36) followed by protein A/15 nm gold.

Biosynthetic Labeling—Cell lines plated into 4-well dishes were allowed to reach 70–80% confluence. After two 20-min rinses with CSFM/air (DMFM/F-12, 25 mM HEPES, pH 7.4, 100 units/ml of penicillin, 100 μg/ml of streptomycin, insulin/transferrin/selenium, and 0.1 mg/ml of BSA), the cells were incubated in medium lacking Met for 5 min. The Met minus medium was replaced with Met minus medium containing [^{35}S]Met (1 mCi/ml; PerkinElmer Life Sciences) for 30 min, and cells were extracted immediately or chased for various times in CSFM/air containing Met. Cells were extracted into TMT for analysis of PAM and into 5 N acetic acid for analysis of proopiomelanocortin (POMC) products (41). Chase media were centrifuged to remove cell debris. PAM was immunoprecipitated using affinity purified JH1761, which binds to PHM. POMC proteins were immunoprecipitated using JH93, which recognizes the amino-terminal region of ACTH. To visualize newly synthesized proteins, immunoprecipitates were resolved by SDS-PAGE; gels were incubated with EnHANCE (PerkinElmer Life Sciences), dried, and subjected to fluorography. Band intensities were quantified using GeneTools software and exposures in the linear range for quantification, and corrected for the number of Met residues in each protein or peptide.

Surface Biotinylation—Cell lines stably expressing PAM-1 or PAM-1/H3A were incubated for 30 min in CSFM/air. Cells were rinsed with HSG buffer (15 mM HEPES, 120 mM NaCl, 2 mM $CaCl_2$, 4 mM KCl, 25 mM glucose, pH 7.5). For assessing steady state plasma membrane localization, surface biotinylation was carried out on ice and all solutions used were pre-

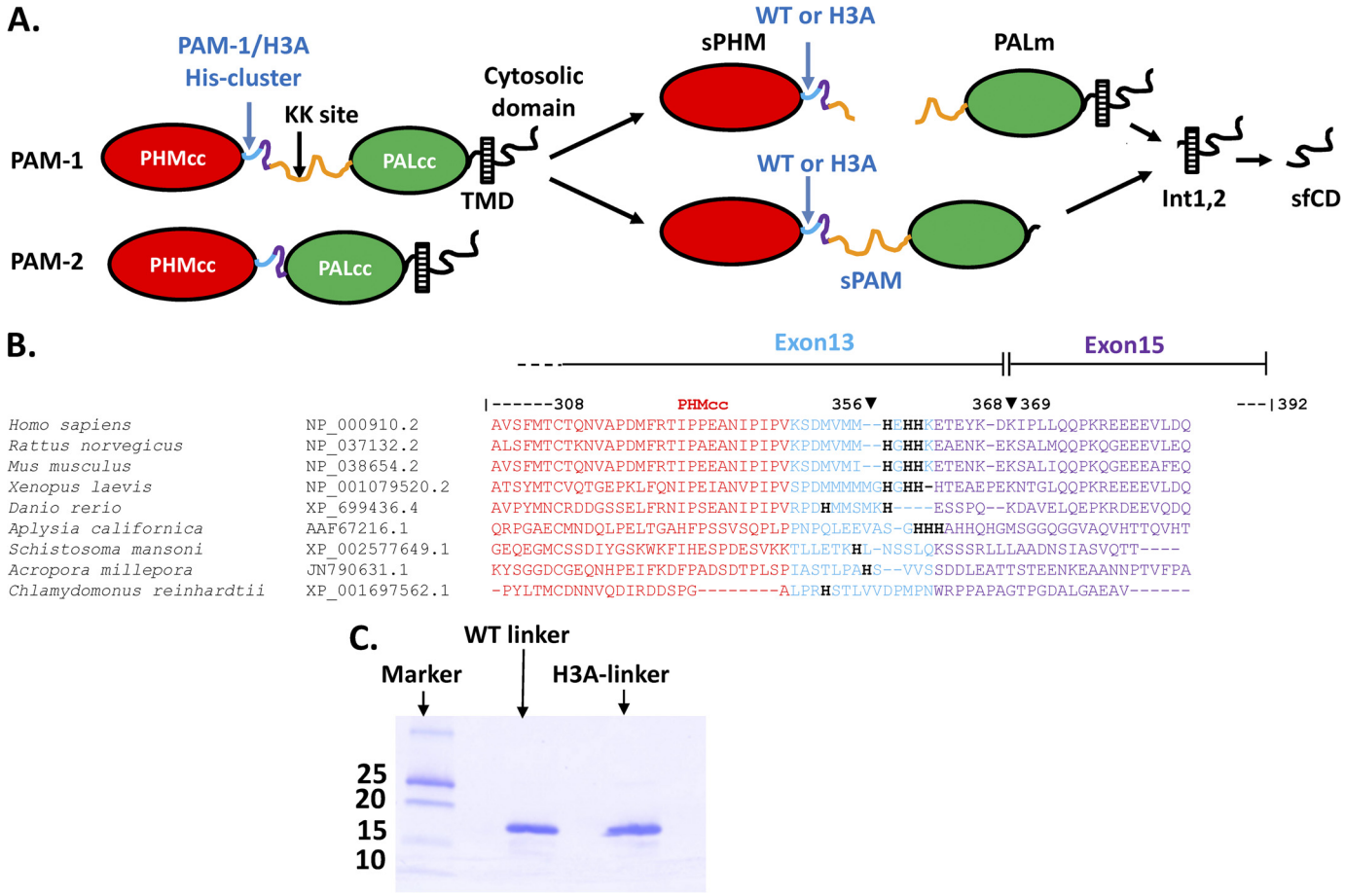

FIGURE 1. **The PAM linker region includes a conserved His cluster.** *A*, the major splice variants of PAM, PAM-1 and PAM-2, are shown; the linker region separating the catalytic cores of PAM-1 (PHMcc and PALcc) is composed of 12 amino acids encoded by the final exon of PHMcc (*light blue*; rat exon 13), 24 amino acids of rat exon 15 (*purple*), and 105 amino acids of exon 16 (*orange*). The linker region in PAM-2 lacks the region encoded by exon 16. *B*, the CLUSTALW sequence alignment for the linker region is shown, with the conserved His cluster indicated; accession numbers are provided. *C*, Coomassie Brilliant Blue R-250 staining shows purified recombinant WT linker and H3A linker.

chilled. For assessment of endocytic trafficking, surface biotinylation was carried out for 10 min at 37 °C. Sulfo-NHS-LC-biotin (1.25 mM) (Pierce) dissolved in HSG buffer was applied on ice or at 37 °C. The reaction was quenched by replacing the buffer with CSFM/air with 2 mg/ml of BSA for 5 min, followed by rinsing in CSFM/air. Cells were either extracted immediately or chased for up to 4 h by incubating in CSFM/air containing 1 mg/ml of BSA. Following extraction into TMT supplemented with protease inhibitors (30 μg/ml of phenylmethylsulfonyl fluoride, 2 μg/ml of leupeptin, 10 μg/ml of α-macroglobulin, and 16 μg/ml of benzamidine) and centrifugation at 14,000 $\times$ *g* for 20 min, clarified lysates and media were incubated with neutravidin beads (25 μl of slurry) (Pierce) for 1 h at 4 °C. Beads were rinsed twice with TMT containing protease inhibitors and once with buffer lacking detergent before eluting the bound proteins into Laemmli sample buffer by heating for 5 min at 95 °C. Eluates were analyzed on 4–15% gradient gels. Band intensities were quantified using GeneTools software and exposures in the linear range for quantification.

RESULTS

His Cluster Imparts pH Sensitivity to Non-catalytic PAM Linker Region—The protease-resistant catalytic core of PHM (PHMcc) is followed by a well conserved cluster of three His residues (Fig. 1, *A* and *B*). This His cluster is included in the final exon (rat exon 13; exon 14 is included only in a rare splice variant) encoding PHMcc and is followed by a poorly conserved, protease-sensitive region encoded by a short exon present in each of the major splice variants of PAM (rat exon 15). The non-catalytic linker region between PHM and PAL can end at exon 15, as in PAM-2, or can include a 315-nt exon (rat exon 16), as in PAM-1 (Fig. 1, *A* and *B*) (42). Exon 16 plays an important role in PAM-1 trafficking and in the ability of PAM-1 to participate in transmembrane signaling (43). To test the hypothesis that these His residues serve as a pH sensor, all three were mutated to Ala. The effects of this change were first evaluated in the context of the linker region alone; purified GST fusion proteins encoding the wild-type linker (WT linker) and the mutated linker (H3A linker) were cleaved and ion exchange chromatography was used to purify both proteins (Fig. 1*C*).

The effect of pH on the far UV CD spectrum of each protein was determined (Fig. 2*A*). At physiological pH, the CD spectrum, with a negative maximum (θ) at 200 nm, revealed the unstructured nature of this region. NMR analysis of ^{15}N-labeled WT linker also indicated that the majority of backbone protons and carbons exhibited chemical shifts characteristic of random-coil configurations at pH 7 (results not shown). The far

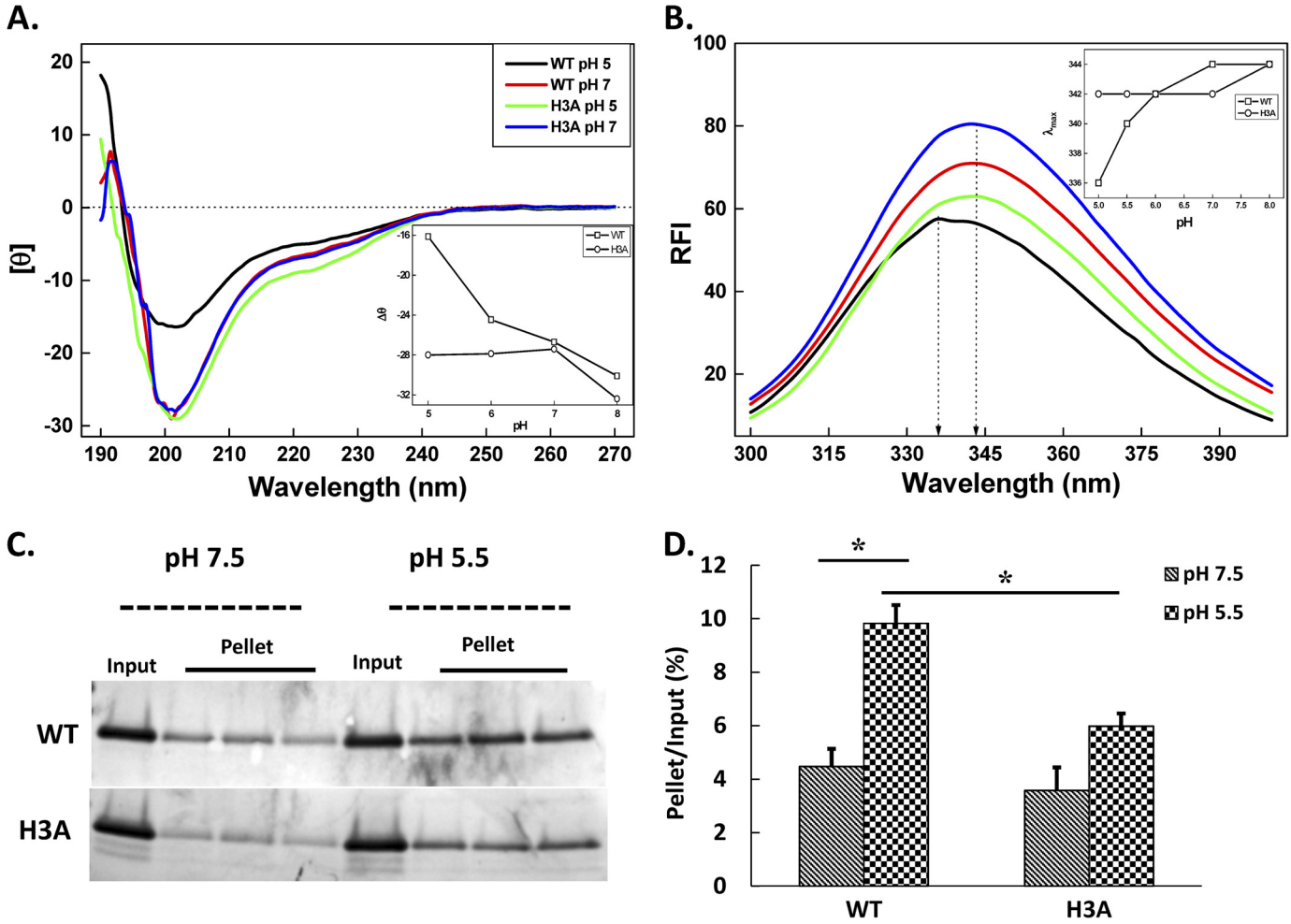

FIGURE 2. **His cluster in WT linker is responsible for its pH-dependent properties.** *A*, a concentrated stock of purified recombinant protein was diluted to 6 μM with 20 mM buffers varying in pH and incubated for 2 h before recording far UV-CD spectra. Representative far UV CD spectra for WT and H3A linker proteins are shown for pH 5.0 and 7.0. *Inset* shows pH-dependent changes monitored by changes in ellipticity (θ) at $\lambda = 200$ nm for the WT and H3A linkers. Values were averaged from three independent experiments. *B*, recombinant proteins were further diluted to assess the pH dependence of their endogenous tryptophan fluorescence. Spectral scans showed a blue shift at acidic pH for the WT linker, indicating a pH-dependent conformational change. *Inset* shows the wavelength of maximum relative fluorescence intensity value (λ_{max}) as a function of pH. *C*, aggregation of recombinant WT and H3A linker was assessed at pH 7.5 or 5.5 in triplicate. Supernatant (an aliquot representing 20% of the sample used (not shown)) and pellet fractions were subjected to SDS-PAGE and stained with Coomassie Brilliant Blue R-250. *D*, the amount of linker protein in each fraction, at pH 7.5 and 5.5, was quantified by densitometric scanning and the amount in the pellets was expressed as a percentage of the input, using lighter exposures in the linear range for quantification (*, $p < 0.01$; $n = 3$).

UV CD spectrum of the WT linker was pH sensitive; $[\theta]_{200\ nm}$ was less negative at pH 5 ($-16{,}100$ deg cm^2 dmol^{-1}) than at pH 7 ($-28{,}150$ deg cm^2 dmol^{-1}). The plot of $[\theta]_{200\ nm}$ *versus* pH revealed a half-maximal effect at approximately pH 6.5, consistent with a role for His protonation in the response. Consistent with this suggestion, the far UV CD spectrum of the H3A linker was not altered when the pH was dropped from pH 7.0 to pH 5.0; $[\theta]_{200\ nm}$ was $-27{,}500$ deg cm^2 dmol^{-1} at both pH values (Fig. 2*A*). The presence of two Trp residues in exon 16 allowed us to use endogenous fluorescence to search for pH-dependent structural changes in the WT linker. The wavelength of the maximum fluorescence intensity peak for WT linker shifted from 344 to 336 nm as the pH was decreased from pH 8.0 to 5.0. The maximum fluorescence intensity peak for the H3A linker was much less sensitive to changes in pH over this range (Fig. 2*B*).

Several secretory granule content proteins aggregate at mildly acidic pH in the presence of calcium, a milieu thought to represent the lumen of the TGN (1). When purified PAM-3, a soluble form of bifunctional PAM was tested for its ability to aggregate through *in vitro* assays, it showed a strong homophilic aggregation (35%, at pH 5.8) when mixed with globin and more extensive aggregation when mixed with adrenal chromaffin granule proteins (55% at pH 5.8) (1). We tested the ability of recombinant WT and H3A linker to aggregate under similar conditions (Fig. 2*C*). A pH 7.5 stock solution of each purified protein was left untouched or titrated to pH 5.5; protein that precipitated during a 1-h incubation at 37 °C was recovered in the pellet fractions after centrifugation. The extent of aggregation and its dependence on pH were diminished in H3A linker assayed in the same manner. As much as 11% of the WT linker precipitated at pH 5.5, whereas only 6% of the H3A linker precipitated under these conditions (Fig. 2*D*).

PAM-1/H3A and PAM-1 in HEK293 Cells—We next introduced the same His mutations into PAM-1 (Fig. 1*A*) and stably expressed the protein in HEK293 cells to evaluate its catalytic activity and in AtT-20 cells to evaluate its processing, trafficking, and ability to alter the function of the regulated secretory

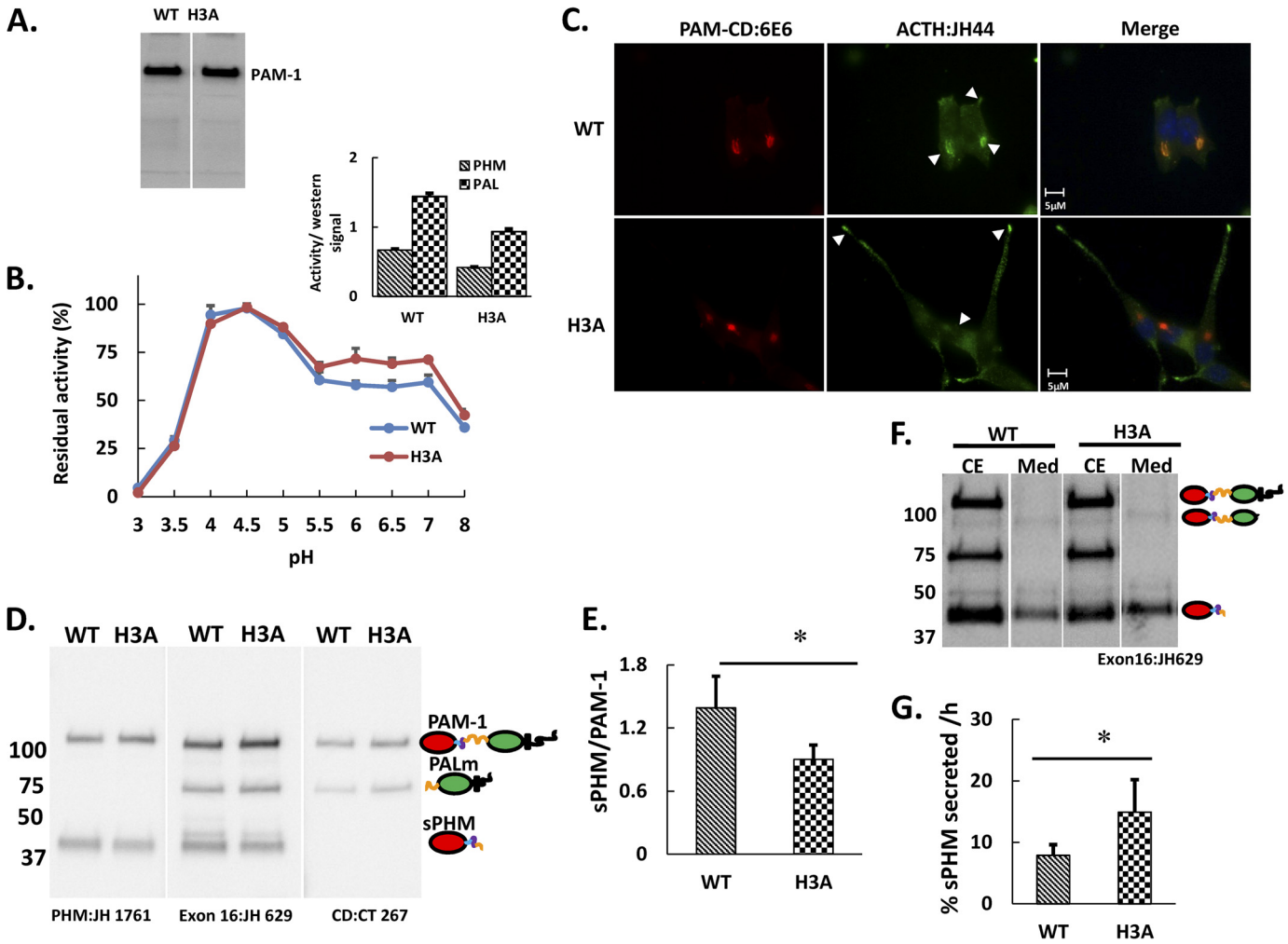

FIGURE 3. **PAM-1/H3A expressed in HEK293 cells is stable and active, and processing of PAM-1 and PAM-1/H3A differs in AtT-20 cells.** *A*, a stably transfected HEK293 cell line expressing PAM-1/H3A was created; the HEK293 line expressing PAM-1 was generated previously (44). Western blot analysis of total cell lysates using an affinity purified antibody specific for PHM (JH 1761) identified a single protein of the same mass (120 kDa) in both samples. *B*, the pH optimum for PHM in lysates of PAM-1 and PAM-1/H3A HEK293 cells was assessed by measuring activity from pH 3.0 to 8.0; maximal PHM activity was set to 100% to facilitate comparison between PAM-1 and PAM-1/H3A. The slight decrease in PHM activity in the pH 5 to 7 range was seen consistently. *Inset*, the specific activities of PHM and PAL in these Triton X-100-solubilized crude particulate fractions at their optimum pH (4.5) was compared by normalizing activity to the amount of PAM protein estimated by Western blot analysis using an antibody to PHM ($n = 3$ for *B* and *inset*). *C*, stable AtT-20 lines expressing PAM-1 or PAM-1/H3A were fixed and stained simultaneously for PAM (6E6, specific for the C terminus of PAM) and ACTH (JH44, specific for the C terminus of ACTH). Cell morphology differed substantially, but PAM was largely localized to the TGN area in both lines; whereas ACTH accumulated in the TGN area in PAM-1 cells, ACTH was more prevalent at the tips of the long processes typically seen in PAM-1/H3A AtT-20 cells. *D*, equal amounts of protein (5 μg) from PAM-1 and PAM-1/H3A cell lysates were fractionated by SDS-PAGE and PAM was visualized using antibodies specific for the indicated regions. Steady state levels of sPHM were lower in PAM-1/H3A cells than in PAM-1 cells. *E*, graph showing the ratio of sPHM to intact PAM-1 in both cell lines was obtained by quantifying blots from six independent experiments (*, $p < 0.05$), using lighter exposures in the linear range for quantification. *F*, AtT-20 cells expressing PAM-1 or PAM-1/H3A were incubated for 1 h in basal medium; cell extracts (*CE*) and spent media (*Med*) were subjected to Western blot analysis using an antibody to PHM. In addition to sPHM, medium samples contained sPAM. *G*, the basal secretion rate of sPHM, which is produced only in the regulated secretory pathway, was calculated from these Western blots (% = 100 × $sPHM_{mdm}/(sPHM_{cell} + PAM\text{-}1_{cell})$) and was significantly higher in PAM-1/H3A cells than in PAM-1 cells (*, $p < 0.05$; $n = 6$).

pathway. Both proteins were expressed at similar levels in the HEK293 clones selected. When cell lysates from PAM-1 and PAM-1/H3A HEK293 cells were probed with a PHM antibody, only a protein the size of full-length PAM-1 (120 kDa) was detected (Fig. 3*A*); HEK293 cells lack the regulated secretory pathway endoproteases that cleave PAM (44). Purified PAM-1 exhibits optimal activity at pH 4.5 (45); PAM-1 solubilized from a crude particulate fraction exhibited a similar pH optimum (Fig. 3*B*). PAM-1/H3A exhibited the same pH optimum, but showed slightly lower activity from pH 5.5 to 7 (Fig. 3*B*). When enzyme activity at pH 4.5, where both proteins show maximal activity, was normalized to the amount of PAM protein present in the lysates based on Western blot signal, PAM-1/H3A exhibited slightly lower PHM and PAL specific activity (Fig. 3*B*, *inset*).

PAM-1/H3A and PAM-1 Are Processed Differently in AtT-20 Cells—When expressed in AtT-20 corticotrope tumor cells, which store the adrenocorticotropic hormone (ACTH) they produce from POMC in mature secretory granules, PAM-1 undergoes endoproteolytic processing in the regulated secretory pathway, generating soluble products that are stored in regulated secretory granules (46–48). AtT-20 cells expressing PAM-1/H3A or PAM-1 were fixed and stained simultaneously for PAM and ACTH (Fig. 3*C*). In both cell lines, PAM staining was largely localized to the perinuclear region in a complex

reticular pattern resembling that of the Golgi complex. ACTH staining in PAM-1/H3A cells was concentrated at the tips of cellular processes (indicated by *arrows*); PAM staining was also detectable at the tips of the processes. As described previously, AtT-20 cells expressing PAM-1 generally lacked extensive cellular processes filled with ACTH-containing secretory granules (32, 50).

The proteolytic processing of PAM-1 and PAM-1/H3A in AtT-20 cells was first compared by analyzing cell lysates using antisera to the PHM, exon 16, and cytosolic domains of PAM (Fig. 3*D*). Although the same major products, sPHM and membrane PAL, were detected, sPHM accounted for a smaller percentage of the total PAM protein in PAM-1/H3A cells than in PAM-1 cells (Fig. 3*E*); because the cleavage generating sPHM occurs in exon 16, sPHM contains the His cluster, whereas membrane PAL does not. The amount of stored sPHM reflects the rate at which it is synthesized *versus* the rate at which it is secreted or degraded. To assess secretion, both cell extracts and spent media were analyzed (Fig. 3*F*); sPHM, which is produced only in the regulated secretory pathway, and sPAM, which is produced primarily in the endocytic pathway, were the major PHM proteins identified in spent media from both cell lines (39). In 60 min, PAM-1/H3A cells secreted 12–18% of their cell content of PHM, whereas PAM-1 cells secreted only 6–9% of their cell content of PHM under basal (not stimulated) conditions (Fig. 3*G*). Increased secretion of sPHM by PAM-1/H3A cells would contribute to their decreased cell content of sPHM.

PAM-1/H3A Trafficking in the Biosynthetic Pathway Is Altered—Metabolic labeling of AtT-20 cells expressing PAM-1 and PAM-1/H3A was used to determine whether their trafficking through the biosynthetic pathway differed; immunoprecipitation with an antibody to PHM allowed quantification of PAM-1, sPHM, and sPAM in cells and spent media (Fig. 4*A*). After a pulse labeling period of 30 min, intact PAM-1 was the only PAM protein detected in both cell lines. sPHM was created only in the regulated secretory pathway (51, 52); the fact that newly synthesized sPHM was first detected after a 1-h chase in both PAM-1 and PAM-1/H3A cells suggests that they entered a cleavage competent compartment (immature secretory granules) at similar times.

Newly synthesized PAM-1/H3A disappeared more quickly than newly synthesized PAM-1 (Fig. 4*B*). This difference was apparent after the 1-h chase and became more marked after the 4-h chase, with half as much newly synthesized PAM-1 remaining in PAM-1/H3A cells. At the end of the 4-h chase, over 40% of the newly synthesized PAM-1 remained intact, whereas less than 25% of the newly synthesized PAM-1/H3A remained intact (Fig. 4*B*). To assess how much of the newly synthesized PAM-1 was converted into smaller products, we plotted total sPHM (cell + mdm) as a % of pulse PAM-1 at each time point. At the end of the 4-h chase period, 82% of the initially labeled PAM-1 had been converted into sPHM, whereas only about 50% of the PAM-1/H3A was recovered as sPHM/H3A (Fig. 4*C*). This result suggests that newly synthesized PAM-1/H3A is subject to degradation.

We next quantified the amount of newly synthesized sPHM recovered from the medium as a percentage of the total sPHM generated by the cells to assess constitutive-like secretion. Newly synthesized sPHM generated from PAM-1/H3A was secreted at a much higher rate than newly synthesized sPHM generated from PAM-1; this difference was especially apparent after the 1-h chase, but was apparent at each chase time (Fig. 4*D*). Lacking the His cluster, sPHM may be less able to aggregate and remain in immature secretory granules.

Bifunctional sPAM, which is generated in the endocytic compartment (Fig. 1*A*), was first detected in the medium of PAM-1 cells after the 2-h chase. Very little sPAM/H3A was produced by PAM-1/H3A cells. Although 5–6% of the newly synthesized PAM-1 was recovered from the medium as sPAM after the 4-h chase, <2% of the newly synthesized PAM-1/H3A was recovered as sPAM/H3A (Fig. 4*E*). To gain a better understanding of the endocytic trafficking of PAM-1/H3A, we turned to surface biotinylation.

H3A Mutation Eliminates the Ability of Internalized PAM-1 to Return to Secretory Granules—In PAM-1 AtT-20 cells, less than 2% of the total PAM-1 is on the surface at steady state (39, 51, 53). Based on previous antibody uptake and surface biotinylation studies, PAM-1 that reaches the plasma membrane is rapidly internalized; whether the internalized PAM-1 protein is recycled or degraded is governed by signals in its cytosolic domain (54–56). We used surface biotinylation to provide a quantitative comparison of the endocytic trafficking of PAM-1 and PAM-1/H3A (Fig. 5). To determine whether the H3A mutation altered the amount of intact PAM-1 or membrane PAL on the cell surface at steady state, cells were exposed to membrane impermeant biotin for 10 min at 4 °C and then lysed. Western blot analysis revealed similar amounts of intact PAM-1 and membrane PAL on the surface of PAM-1 and PAM-1/H3A cells at steady state (Fig. 5, *A* and *B*).

To compare the fate of internalized PAM-1 and PAM-1/H3A, cells incubated with cell-impermeant biotin for 10 min at 37 °C were quenched and harvested immediately or chased in growth medium for up to 4 h before extraction (Fig. 5, *C* and *D*). As observed previously, almost half of the biotinylated PAM-1 and membrane PAL remained intact after a 4-h chase; in contrast, only about 10% of the biotinylated PAM-1/H3A remained intact and there was no detectable signal for membrane PAL after the 2-h chase period (Fig. 5*D*). As seen previously, biotinylated PAM-1 was converted into sPAM and sPHM; conversion of biotinylated PAM-1 into biotinylated sPHM requires its return to the regulated secretory pathway (Fig. 5*C*) (16, 39). In contrast, biotinylated PAM-1/H3A simply disappeared; no production of biotinylated sPAM/H3A or biotinylated sPHM/H3A was detectable.

Alkalinizing Agents Show Differential Effects on PAM-1 and PAM-1/H3A—To determine whether these three His residues are involved in the ability of PAM-1 to respond to intraluminal pH, we dissipated the pH gradients along the secretory and endocytic pathways by incubating cells with medium containing weak bases (NH_4Cl and methylamine) or concanamycin A, an inhibitor of the V-ATPase responsible for acidifying luminal compartments. Although luminal pH is elevated to a similar extent by both treatments, V-ATPase inhibitors exert additional effects (35). NH_4Cl/methylamine treatment had no discernible effect on the morphology of PAM-1 or PAM-1/H3A AtT-20 cells. As previously reported, PAM-1 cells exposed to

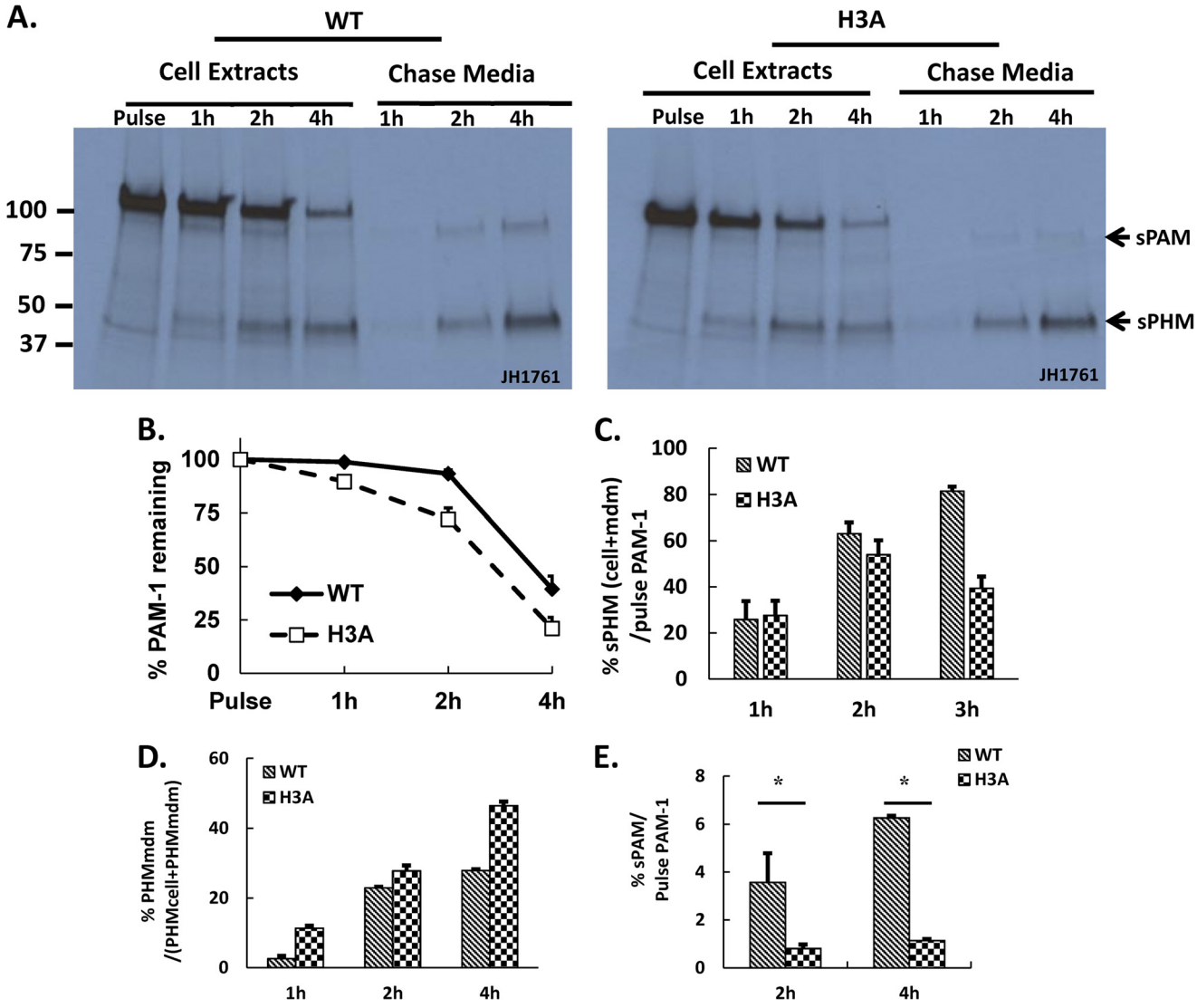

FIGURE 4. **Pulse-chase metabolic labeling demonstrates altered metabolism of newly synthesized PAM-1/H3A.** *A*, four matched wells of AtT-20 cells expressing PAM-1 or PAM-1/H3A were incubated with medium containing [^{35}S]Met for 30 min and either harvested immediately (*Pulse*) or after a 1-, 2-, or 4-h incubation in medium lacking [^{35}S]Met (*Chase*; both cells and media were analyzed). PAM proteins immunoprecipitated using an antibody to PHM were fractionation by SDS-PAGE and quantified using fluorography. sPHM and sPAM were the major proteolytic cleavage products (indicated by *arrows*) in both cell types. *B*, total recovery was calculated by taking 120-kDa PAM present after the pulse as 100%. *C*, the turnover rate of freshly made PAM-1 was calculated by obtaining the ratio of sPHM (cell + mdm) at each chase time to the amount of labeled PAM-1 after the pulse, adjusting for the number of methionine residues in each domain of PAM, and using lighter exposures in the linear range for quantification; data from three experiments were averaged. *D*, secretion of newly synthesized sPHM was calculated with reference to the total amount of sPHM present at that time (cells plus medium). *E*, secretion of newly synthesized sPAM was calculated by dividing $sPAM_{mdm}$ (0–4 h) by $PAM\text{-}1_{cell}$ after the pulse (*, $p < 0.05$). *B–E* are averages of three experiments.

concanamycin A formed mixed organelles, which contain components of lysosomes and secretory granules (35); PAM-1/H3A AtT-20 cells exhibited a distinctly different morphological response to concanamycin A.

Lysates and spent media prepared from control and drug-treated cells were examined using an antibody specific for the PHM domain of PAM (Fig. 6*A*). Most notable was the appearance of increased amounts of sPAM in lysates prepared from concanamycin A-treated PAM-1 AtT-20 cells; this response was not seen in PAM-1/H3A cells and was not seen in either cell line in response to NH_4Cl/methylamine treatment (Fig. 6*B*). The sPHM/PAM-1 ratio in PAM-1 cells was reduced by NH_4Cl/methylamine and by concanamycin; as noted above, this ratio was lower in PAM-1/H3A cells and was not altered by either treatment (Fig. 6*C*). Decreasing intracellular pH gradients with NH_4Cl/methylamine or V-ATPase inhibitors reduced secretion of sPHM by PAM-1 cells; secretion of sPHM by PAM-1/H3A cells was also inhibited by concanamycin A (Fig. 6*D*). The different responses observed in PAM-1 and PAM-1/H3A cells reflect both the change in luminal pH and the role of the V-ATPase in additional events such as membrane fission and fusion (35).

H3A Results in Reduced sf-CD Production—sPAM is thought to be formed exclusively in the endocytic pathway; the other product of the cleavage that generates sPAM can serve as a substrate for regulated intramembrane proteolysis by γ-secretase, releasing a soluble fragment of PAM-CD referred to as sf-CD (Fig. 1*A*) (15, 16, 39). The failure of PAM-1/H3A AtT-20 cells to generate sPAM/H3A from internalized PAM-1/H3A led us examine sf-CD production. Detection of sf-CD in PAM-1

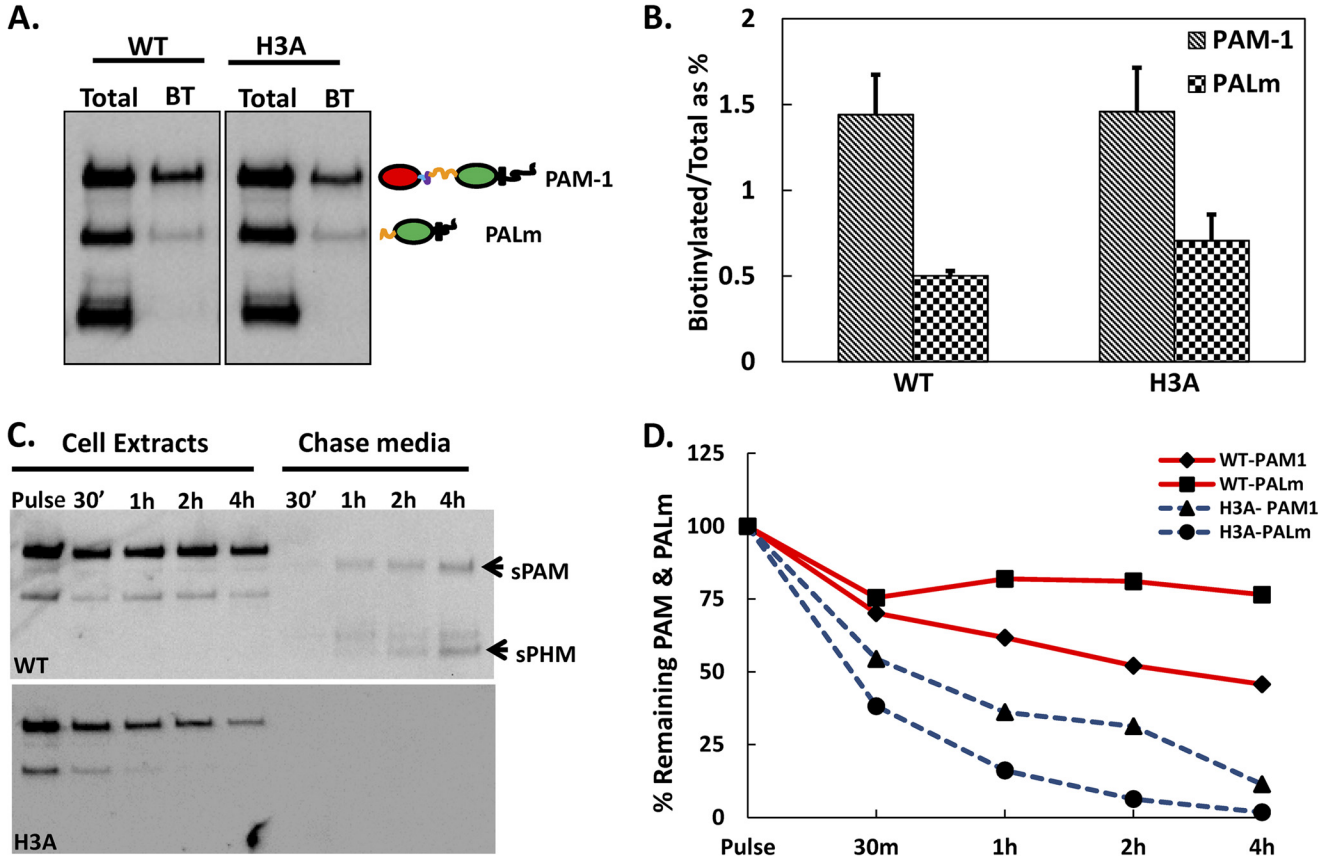

FIGURE 5. **Internalized PAM-1/H3A is degraded.** *A*, cells chilled to 4 °C were exposed to cell-impermeant activated biotin for 10 min; the reaction was quenched and biotinylated proteins isolated from cell lysates were fractionated and probed for PAM using affinity purified exon 16 antibody. The total lanes represent 0.5% of the amount analyzed after biotinylation (*BT*). *B*, graph shows the ratio of biotinylated intact PAM-1 and membrane PAL to total PAM-1 or membrane PAL at steady state in both cell types, using lighter exposures in the linear range for quantification. *C*, cells kept at 37 °C were exposed to cell impermeant-activated biotin for 10 min; the reaction was quenched and cells were harvested or chased in growth medium for the indicated amount of time; biotinylated proteins were isolated from cell extracts and spent media, fractionated, and probed for PAM using the exon 16 antibody. *Arrows* indicate secreted products produced from biotinylated PAM-1. *D*, biotinylated PAM-1 and membrane PAL remaining at each chase was plotted as a percentage of the total present after the pulse. *B* and *D* are averages of two experiments.

AtT-20 cells is facilitated by preincubation with MG132, a proteosomal inhibitor (15). Lysates prepared from control and MG-132-treated AtT-20 cells expressing PAM-1 or PAM-1/H3A were examined using an antibody specific for the C terminus of the cytoplasmic domain of PAM (Fig. 7*A*). Intermediates 1 and 2, which arise from cleavages between PALcc and the transmembrane domain, were detected in both lysates in the absence or presence of MG-132; sf-CD was detected in MG-132-treated PAM-1 cells, but not in MG-132-treated PAM-1/H3A cells. Levels of the intermediates and sf-CD in the absence and presence of MG-132 were quantified (Fig. 7*B*). The presence of MG132 had a more pronounced effect on levels of intermediate 2 and sf-CD, products thought to be generated in the endocytic pathway, and a smaller effect on intermediate 1, which is thought to be generated in the regulated secretory pathway (15). The decreased levels of intermediate 2, the substrate for γ-secretase, in PAM-1/H3A cells could contribute to decreased production of sf-CD (Fig. 7*B*).

Previous ultrastructural studies using protein A/gold conjugates of antisera to the luminal domains of PAM and PAM-1 AtT-20 cells demonstrated clathrin-mediated internalization of PAM·antibody complexes followed by the regulated entry of PAM-1·antibody complexes into the intraluminal vesicles of multivesicular bodies (39, 51). The same protocol was used to examine the internalization of PAM·antibody complexes by PAM-1/H3A AtT-20 cells. Despite the fact that the percentage of PAM-1 and PAM-1/H3A on the cell surface at steady state is identical (Fig. 5, *A* and *B*), internalization of PAM·antibody complexes was decreased dramatically in PAM-1/H3A cells. After internalization for 20 min of the PAM·antibody complexes, the multivesicular bodies of PAM-1 cells contained more than four times as many gold particles as the multivesicular bodies of PAM-1/H3A cells (905 gold particles in 73 multivesicular bodies in PAM-1 cells *versus* 202 gold particles in 73 multivesicular bodies in PAM-1/H3A cells). The multivesicular bodies accumulating PAM antibody in the PAM-1/H3A cells had a smaller transection diameter than seen in PAM-1 cells (310 ± 9 nm for PAM-1 cells to 271 ± 7 nm for PAM-1/H3A cells ($p < 0.005$)). Despite these changes, trafficking of the PAM·antibody complexes that reached the multivesicular bodies into intraluminal vesicles was not altered in PAM-1/H3A cells (Fig. 7*C*).

To further explore the fate of PAM·antibody complexes internalized by PAM-1/H3A cells, the chase time was reduced to 10 min (Fig. 7*D*). The morphology of the early endosomes containing PAM·antibody complexes was not altered in PAM-

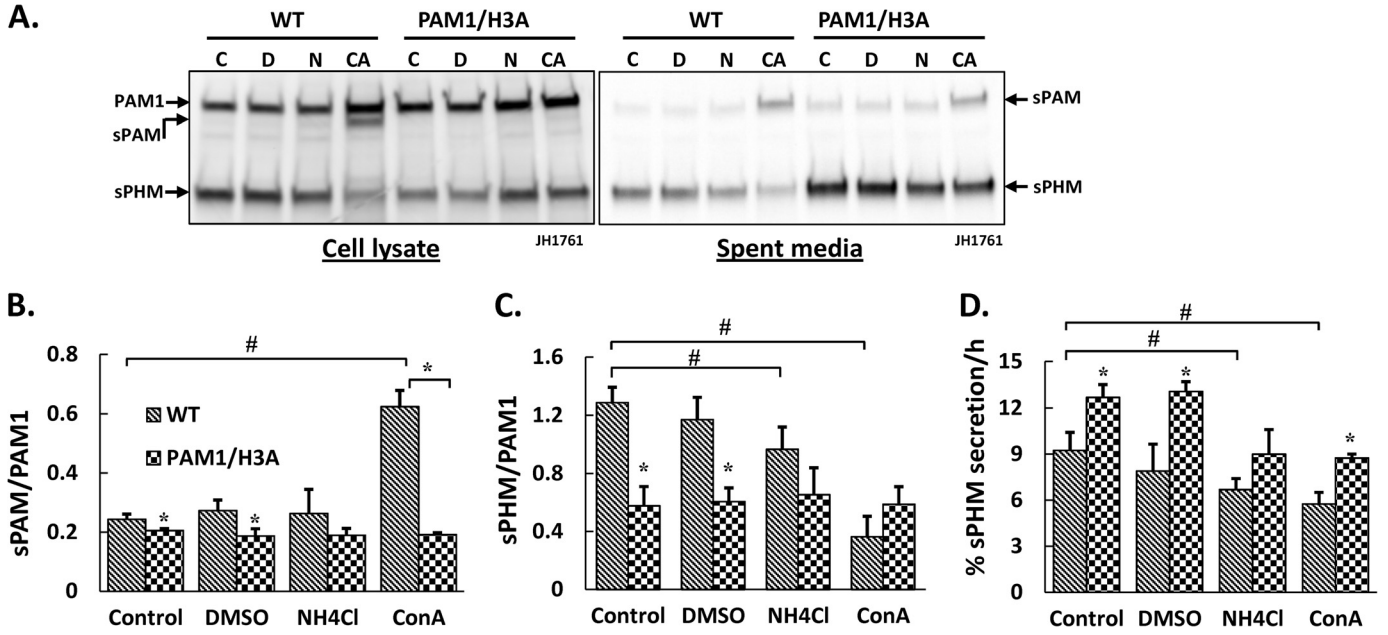

FIGURE 6. **The processing and trafficking of PAM-1/H3A is less sensitive to dissipation of intracellular pH gradients than PAM-1.** *A*, cells were treated with alkalinizing agents or concanamycin A for 24 h and lysates were collected into TMT when spent medium was harvested. For cell lysates, equal amounts of protein (5 μg) from control (*C*), dimethyl sulfoxide (*DMSO*) vehicle (*D*), 2.5 mM ammonium chloride and 5 mM methylamine (*N*) and 1 nM concanamycin A (*CA*)-treated cells was fractionated by SDS-PAGE; an aliquot (1%) of the spent medium was also analyzed. PAM was visualized using an antibody specific to PHM (*, nonspecific band). Processing was evaluated by plotting the sPAM/PAM-1 (*B*) and sPHM/PAM-1 (*C*) ratios from duplicate samples from two independent experiments; *error bars* show range. *D*, the amount of sPHM collected in each 24-h medium sample was compared with the amount of sPHM in the cell lysate; data are expressed as % sPHM secreted/h. #, treatment effect significant for PAM-1, $p < 0.05$; *, PAM-1/H3A different from PAM-1 for that treatment group, $p < 0.05$.

1/H3A cells. Although the diminished levels of PAM·antibody complex observed in PAM-1/H3A cells correlate well with the rapid loss of the biotinylated PAM-1/H3A and biotinylated membrane PAL/H3A, the trafficking steps involved in their rapid disappearance are unclear. In both AtT-20 cells and primary rat pituitary cells, sf-CD has been shown to enter the nucleus (16, 39), where it is thought to alter gene expression, contributing to alterations in cytoskeletal organization and control of the regulated secretory pathway attributed to expression of PAM-1. Because of its reduced ability to produce sf-CD, expression of PAM-1/H3A would be predicted to lack the ability to alter secretory pathway function in AtT-20 cells.

Expression of PAM-1/H3A Does Not Alter AtT-20 Cell Morphology—Analysis of AtT-20 cells engineered to express PAM-1 upon induction with doxycycline established the ability of this integral membrane protein to alter cytoskeletal organization and control of the regulated secretory pathway (49). The morphology of AtT-20 cells stably expressing PAM-1/H3A resembled non-transfected AtT-20 cells more than PAM-1 AtT-20 cells (Fig. 8*A*). Unlike non-transfected AtT-20 cells, which generally adopt an elongated spindle shape, PAM-1 AtT-20 cells tend to grow in groups of 10–15 polygonal cells (32). AtT-20 cells expressing PAM-1/H3A at similar levels had the spindle-shaped morphology of non-transfected AtT-20 cells (Fig. 8*A*). Quantification of cell area and cell elongation (L/W ratio) revealed no change in cell area, but a striking decrease in L/W ratio only in PAM-1 AtT-20 cells (Fig. 8*B*). Consistent with the diminished ability of PAM-1 AtT-20 cells to engage in regulated secretion of POMC products, transmission EM studies previously revealed an accumulation of secretory protein in the TGN area (Fig. 8*C*, *left*); the *black arrows* mark a cisternal structure full of dense material previously shown to include PAM and POMC products (56). Similar analysis of AtT-20 cells expressing PAM-1/H3A revealed a normal Golgi structure with its trans-most cisternae free of accumulated secretory products. In contrast, the morphology of mature secretory granules seen near the plasma membrane was indistinguishable in AtT-20 cells expressing PAM-1 and PAM-1/H3A (Fig. 8*C*, *right*).

To compare ACTH localization on a whole cell level, we fixed non-transfected AtT-20 cells and AtT-20 cells expressing PAM-1 or PAM-1/H3A and visualized mature ACTH (the antibody used does not detect intact POMC) and GM130, a *cis*-Golgi marker (Fig. 9) (57). As expected, mature ACTH accumulated in puncta located at the tips of the spindle-shaped non-transfected AtT-20 cells; line scans revealed some ACTH in the Golgi region. In contrast, ACTH accumulated in the Golgi region of AtT-20 cells expressing PAM-1. In AtT-20 cells expressing PAM-1/H3A, ACTH accumulated in punctate structures located at the tips of cellular processes, with little ACTH signal in the Golgi region (Fig. 9*A*, *right*). The relative fluorescence intensity graphs revealed significantly different patterns for ACTH in AtT-20 cells expressing PAM-1 and PAM-1/H3A (Fig. 9*B*). When the line scans were subjected to quantification, it was clear that the steady state distribution of ACTH in PAM-1/H3A cells resembled the pattern in non-transfected AtT-20 cells, where mature ACTH accumulated in the tips of the processes (Fig. 9*C*).

POMC Processing and Secretion Are Not Inhibited in AtT-20 Cells Expressing PAM-1/H3A—Pulse-chase metabolic labeling followed by immunoprecipitation with an antibody that recognizes the N-terminal region of ACTH was used to assess POMC

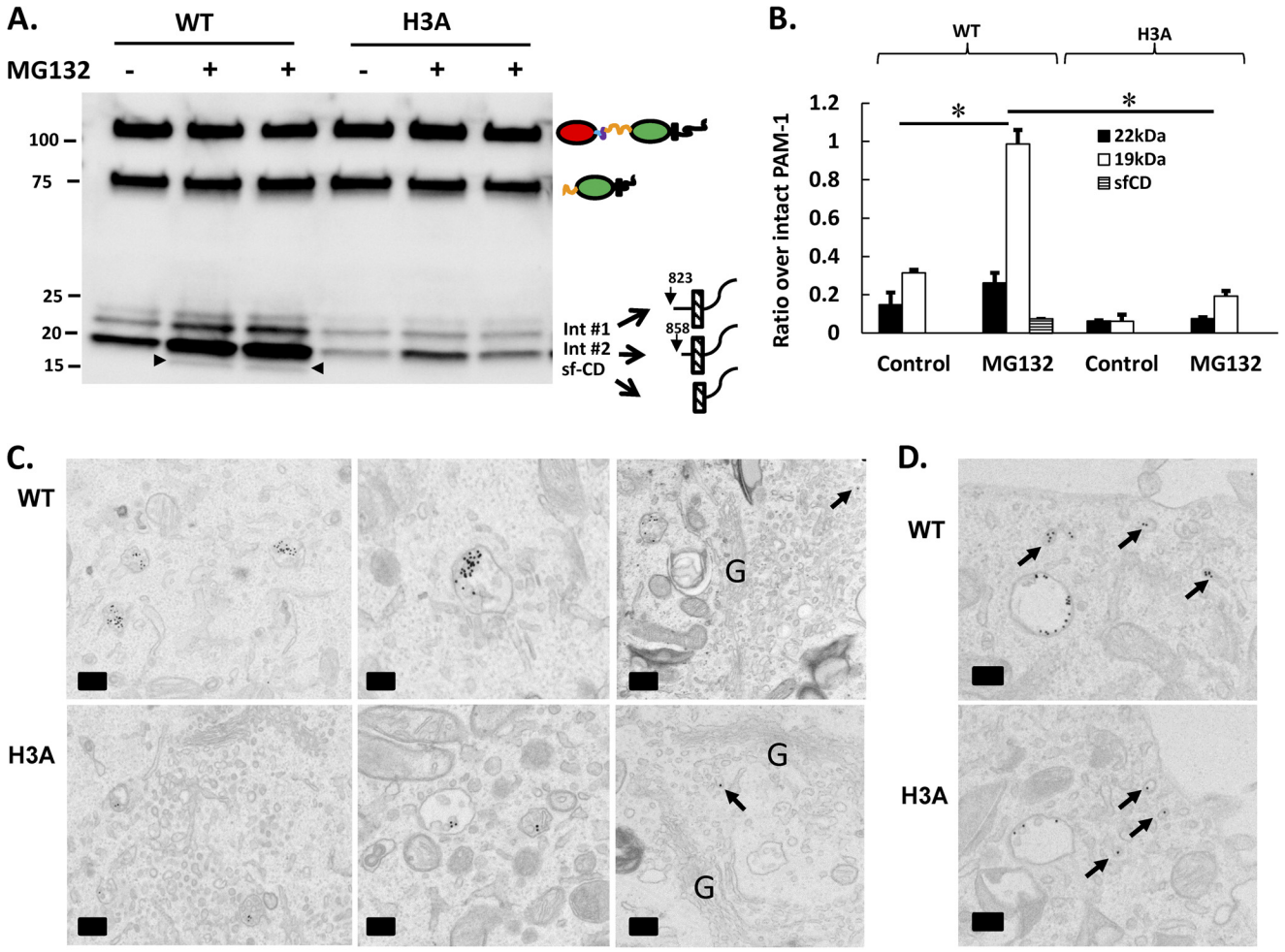

FIGURE 7. **Negligible amounts of sf-CD are generated from PAM-1/H3A.** *A*, AtT-20 cells expressing PAM-1 or PAM-1/H3A were harvested under control conditions or after a 4.5-h pre-treatment with MG132; cell lysates were analyzed using an antibody specific for the C terminus of PAM. *Arrowheads* indicate bands corresponding to sf-CD. Two treated samples for each cell type are compared with controls. *B*, signals for sf-CD, 19- and 22-kDa intermediates were quantified and expressed as a percentage of intact 120-kDa PAM-1, using lighter exposures in the linear range for quantification (*, $p < 0.05$, $n = 6$). *C*, PAM-1 and PAM-1/H3A AtT-20 cells were exposed to PAM antibody·protein A/gold complex for 15 min at 4 °C; after a 20-min chase, cells were fixed and PAM antibody·protein A/gold complexes were localized using transmission electron microscopy. In both cell lines, PAM antibody internalized for 20 min accumulated in multivesicular bodies; some gold particles were detected in the TGN (*arrows*). The proportion of gold particles at the outer membrane *versus* intraluminal vesicles of multivesicular bodies was not cell-type specific. *D*, PAM antibody·protein A/gold complexes were examined after a 10-min chase; for both cell lines, PAM·antibody complexes were seen in early endosomes and recycling tubules (*arrows*). *Scale bar* = 200 nm.

processing in non-transfected AtT-20 cells and in AtT-20 cells expressing PAM-1 or PAM-1/H3A. The ordered, sequential cleavage of newly synthesized POMC at pairs of basic residues generates ACTH biosynthetic intermediate followed by ACTH, which is found in a glycosylated and non-glycosylated form (Fig. 10) (41, 58). Cells incubated in medium containing [^{35}S]Met for 30 min were harvested immediately or chased for 1, 2, and 4 h; chase cell extracts and media were analyzed. POMC remains intact at the end of the 30-min pulse; partial glycosylation of ACTH generates the two forms observed (41). Extensive cleavage of newly synthesized POMC occurred in all three cell lines during the first hour of chase, with the appearance of ACTH biosynthetic intermediate, glycosylated ACTH, and ACTH. Although control AtT-20 cells store a significant amount of newly synthesized ACTH, PAM-1 AtT-20 cells do not; instead, secretion of newly synthesized POMC and ACTH biosynthetic intermediate occurs (41). In AtT-20 cells expressing PAM-1/H3A, newly synthesized POMC was converted into ACTH, which was stored in the cells (Fig. 10*A*).

Another striking effect of PAM-1 expression in AtT-20 cells is its ability to diminish secretagogue-stimulated release of POMC products (49, 56). Western blot analysis of 16-kDa fragment secretion was used to assess the ability of non-transfected AtT-20 cells and AtT-20 cells expressing PAM-1 or PAM-1/H3A to respond to stimulation with $BaCl_2$, which mimics increased intracellular Ca^{2+} levels. Robust stimulation of the 16-kDa fragment secretion was apparent in non-transfected AtT-20 cells and in AtT-20 cells expressing PAM-1/H3A; release of the 16-kDa fragment by AtT-20 cells expressing PAM-1 was much less responsive to secretagogue treatment (Fig. 10*B*).

When these Western blots from two independent experiments were quantified, the steady state signal for the 16-kDa fragment in WT PAM-1 cells was significantly lower than in both non-transfected and PAM-1/H3A cells (Fig. 10*C*), reflecting the disruption of regulated secretion in them. This apparent decrease in the steady state content of POMC products in WT PAM-1 cells led to a reduced accumulation of 16-kDa fragment in the medium after a 30-min barium stimulation (Fig. 10*D*).

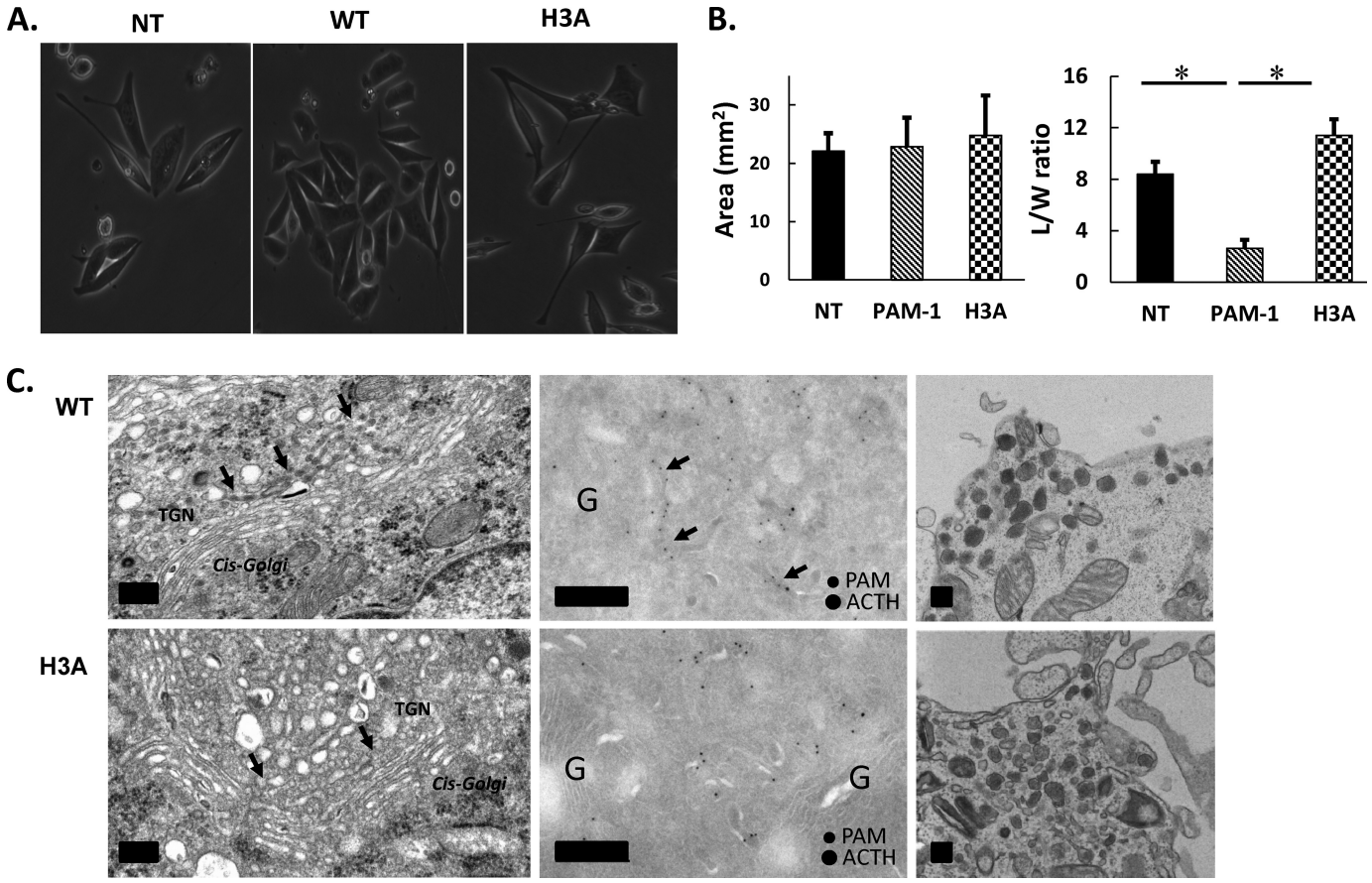

FIGURE 8. **Morphology of AtT-20 cells expressing PAM-1/H3A.** *A*, phase image of non-transfected (*NT*), WT PAM-1, and PAM-1/H3A expressing AtT-20 cells shows altered cell morphology. *B*, cell area and length/width ratio were quantified, demonstrating that PAM-1/H3A cells were more similar to non-transfected AtT-20 cells than to PAM-1 AtT-20 cells (*, $p < 0.05$, $n = 5$). *C*, transmission EM shows condensation of protein in the cisternae of the TGN in WT PAM-1 cells; this phenomenon was not observed in PAM-1/H3A cells (*left*). Immunolabeling of cryosections shows PAM and ACTH in a trans-most cisterna of the TGN in a PAM-1 cell (*arrows*); PAM staining in the tubulovesicular structures of the TGN was similar in WT PAM-1 and PAM-1/H3A cells (*middle*). Mature secretory granules at the tips of the cells were similar in both lines (*right*). *Scale bar* = 200 nm.

DISCUSSION

Histidine Cluster Imparts pH Sensing Capability to PAM Linker—As the only amino acid with a titratable side chain pK_a in the physiological range, His residues are known to play a key role in the many cellular events regulated by pH; clusters of His residues or single His residues can serve this purpose. A single His residue controls the interaction of lysosomal membrane protein type 2 (LIMP-2) with its lysosomal cargo protein, β-glucocerebrosidase (60), and a single His residue serves as the pH sensor that regulates furin activation in the secretory pathway (61). As the key regulator of luminal pH, the vacuolar H^+-ATPase would be expected to sense pH and relay this information to the appropriate cytosolic machinery (18, 19). Five of the 21 luminal His residues in the a2-subunit of mouse V-ATPase are needed to sense endosomal pH and trigger the conformational change that transmits this information to its cytoplasmic domain (18). Similarly, α viruses like Semliki Forest virus use a His residue to regulate the low pH-dependent refolding of E1 to trigger virus-membrane fusion (62).

In earlier studies, we used epitope masking to determine that soluble and membrane forms of PAM exhibit a conformational change between pH 7.5 and 5.5 (63). The presence of a conserved cluster of His residues in the linker region of mammalian and *Xenopus* PAM led us to investigate the possibility that this region could serve as a pH sensor; if the single His residues found in *Acropora*, *Schistosoma*, and *Chlamydomonas* PAM serve a similar function, this role is ancient (Fig. 1). Although the structures of the catalytic cores of rat PHM and PAL have been determined, far UV CD and NMR analyses both indicate that its linker region is unstructured in the buffers used and attempts to crystallize bifunctional PAM have not yet met with success.

Based on a decrease in negative ellipticity and a blue-shift in the λ_{max} for intrinsic Trp fluorescence, recombinant wild-type PAM linker responds to a shift from pH 7 to 5; this response is lost in the H3A linker. Unfolding and refolding studies of bovine serum albumin showed a similar dip in ellipticity at acid pH, reflecting protein compressibility (64). The decreased negative ellipticity and blue-shifted λ_{max} observed upon protonation of His residues in the WT linker suggest that its structure is more tightly packed at low pH (61).

The decrease in luminal pH as proteins move from the Golgi through the TGN and into immature secretory granules is known to contribute to the aggregation of cargo proteins entering the regulated secretory pathway (63, 65). Purified WT linker is more susceptible to low pH-induced aggregation than H3A linker, suggesting that it could contribute to this process. In test tube assays, purified soluble PAM-3 undergoes pH-dependent aggregation (1). PAM in pituitary and adrenal lysates, which

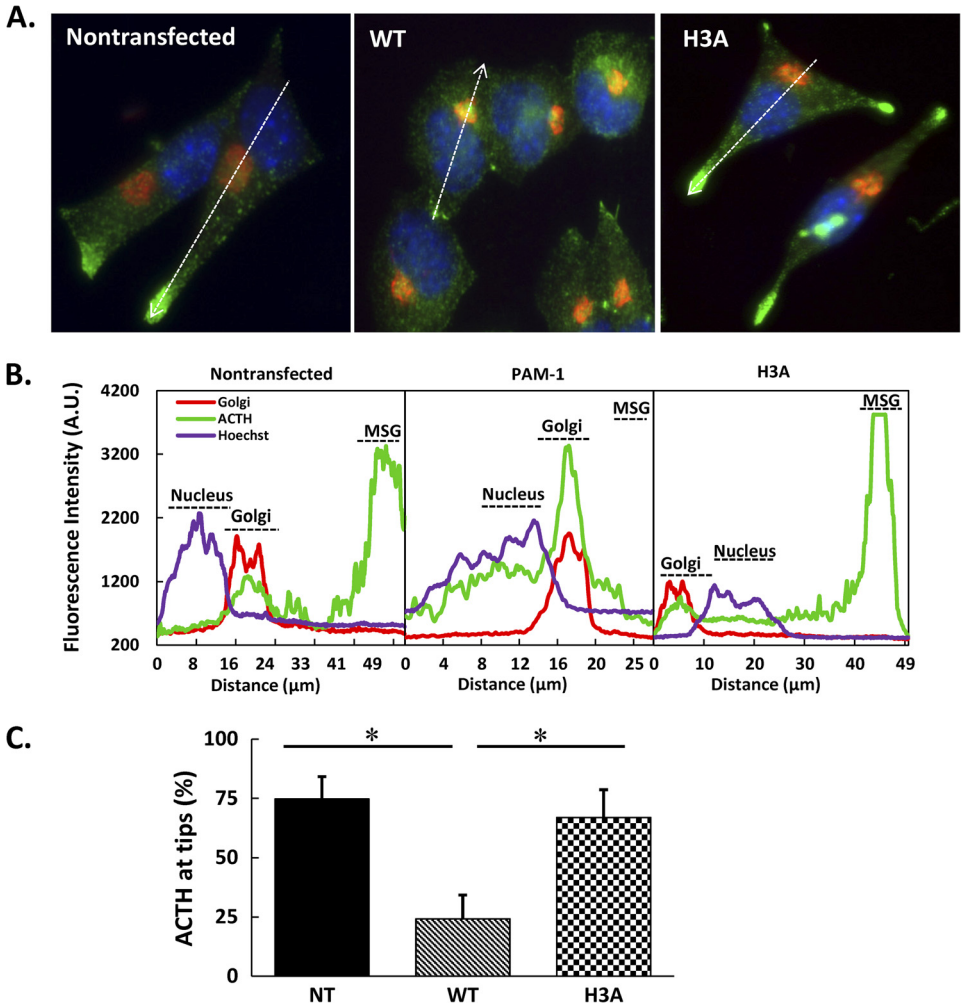

FIGURE 9. **ACTH localization in PAM-1/H3A AtT-20 cells.** *A*, steady state distribution of ACTH was compared with that of a cis-Golgi marker (GM130) in non-transfected (*NT*), WT PAM-1 and PAM-1/H3A AtT-20 cells. As observed previously, ACTH accumulated in the Golgi region in PAM-1 AtT-20 cells and at the tips of processes in non-transfected cells (*arrows*). In PAM-1/H3A AtT-20 cells, ACTH accumulated at the tips of cellular processes (*arrows*). *B*, line scan through the long axis of each cell allowed quantification of differences in steady state localization of ACTH in these three cell types. *C*, for each cell type, line scans ($n = 10$) were used to calculate the % ACTH signal accumulated at the tips of cellular processes (*, $p < 0.01$).

interacts with other cargo proteins, also aggregates at low pH (1). In the presence of trifluoroethanol, WT linker acquires more helical structure (data not shown); additional studies will be required to determine the effect of pH on the structure of the linker region when constrained by its attachment to PHM and PAL in PAM-3 and PAM-1.

Like PAM-1, PAM-1/H3A exhibited maximal PHM activity at pH 4.5, although its specific activity was diminished by a factor of about two (Fig. 3); the decrease in specific activity could reflect an increased level of immature PAM-1/H3A protein due to its limited endocytosis. It is our hypothesis that PAM-1/H3A, like the H3A linker, loses the ability to respond normally to pH values that drop below pH 7.

PAM-1/H3A Is Less Sensitive to pH Gradient Dissipation Than PAM-1—Acidification of secretory granules is crucial to the proteolytic processing of prohormones and their processing enzymes (35, 66, 67). A clear role for the PAM-1 His cluster in responding to luminal pH is supported by the ability of both NH_4Cl/methylamine and concanamycin treatment to diminish sPHM levels in PAM-1, but not in PAM-1/H3A, cells (Fig. 6*C*). The V-ATPase acts as a proton pump and as a pH sensor, relaying luminal pH information to cytosolic interactors (17, 18, 37, 49, 59). The interaction of the V-ATPase with Arf6 and ARNO depends on luminal acidification and is important for budding and endosome-derived carrier-vesicle formation (19). The increased accumulation of sPAM in concanamycin, but not in NH_4Cl/methylamine, treated PAM-1 cells indicates that this response is not solely due to altered luminal pH; concanamycin was without effect on sPAM levels in PAM-1/H3A cells, perhaps because internalized PAM-1/H3A enters a degradative compartment instead of entering multivesicular bodies (Fig. 6, *A* and *B*). PAM-1/H3A cells secreted sPHM more quickly than PAM-1 cells, but sPHM secretion by both cell lines was decreased following prolonged exposure to NH_4Cl/methylamine or concanamycin (Fig. 6*D*); this result indicates that additional regions of PAM-1 contribute to its pH sensitivity.

Role of His Cluster in PAM Trafficking—Metabolic labeling studies indicated that newly synthesized PAM-1 and PAM-1/H3A first enter a cleavage competent compartment at the same time. Newly synthesized PAM-1/H3A is more likely to undergo degradation and soluble PHM/H3A is more likely to undergo basal secretion. Earlier studies demonstrated that PAM-4, a

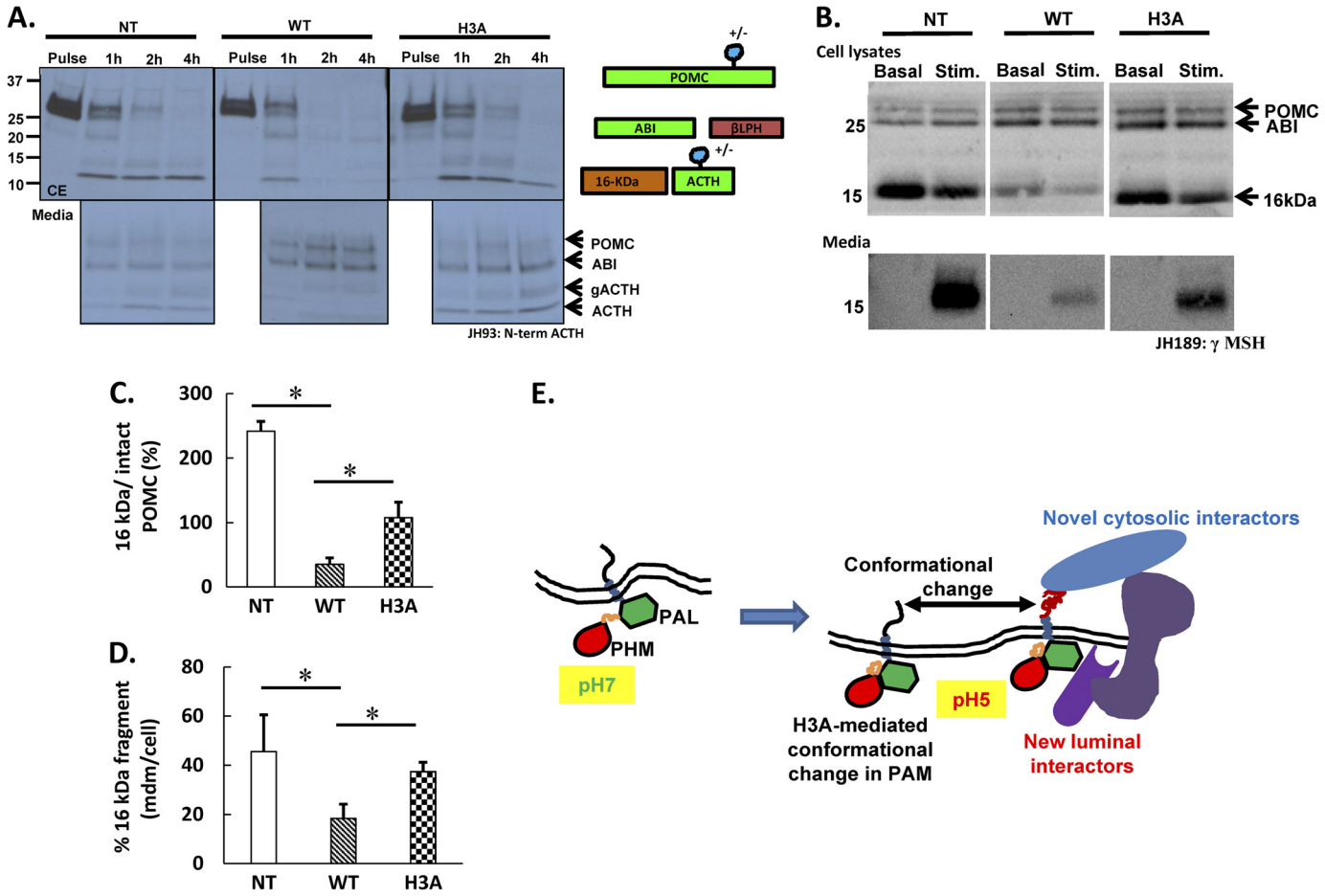

FIGURE 10. **POMC processing and secretion proceed normally in AtT-20 cells expressing PAM-1/H3A.** *A*, non-transfected (*NT*), WT PAM-1, and PAM-1/H3A AtT-20 cells were incubated with [^{35}S]Met for 30 min; cells and media were harvested immediately (*Pulse*) or after a 1-, 2-, or 4-h chase; ACTH-containing peptides were immunoprecipitated using an antibody specific for the N-terminal region of ACTH (JH93). Expression of PAM-1 reduced POMC cleavage and increased secretion of ACTH biosynthetic intermediate (*ABI*). In non-transfected and PAM-1/H3A AtT-20 cells, POMC was cleaved into ACTH and glycosylated ACTH (*gACTH*), which were both secreted. A schematic showing the major POMC cleavage products is shown; the antibody used for immunoprecipitation detects POMC, ABI, gACTH, and ACTH. *B*, non-transfected, PAM-1 and PAM-1/H3A AtT-20 cells were incubated with control medium (*Basal*) or challenged with medium containing 2 mM $BaCl_2$ for 30 min; cell lysates and aliquots of medium were subjected to Western blot analysis using an antibody specific for the γMSH region of POMC (JH189). $BaCl_2$ stimulated the secretion of the 16-kDa fragment by non-transfected and PAM-1/H3A AtT-20 cells; in contrast, little stimulation of the 16-kDa fragment secretion was observed in PAM-1 AtT-20 cells. *C*, JH 189 signals at steady state in the cell extracts for intact POMC and 16-kDa fragment were quantified and expressed as percentage of 16-kDa fragment to intact POMC; $n = 3$. *D*, graph shows percentage of 16-kDa fragment in the medium to its basal cell content in non-transfected, WT, and H3A cells. Experiments were repeated twice with duplicates. Data were analyzed using two-tailed *t* test assuming unequal variance; *error bars* indicate S.D. *, $p < 0.05$, $n = 3$. *E*, a pH-dependent conformational change in the luminal domain of PAM alters the ability of its unstructured, multiply phosphorylated C-terminal region to interact with cytosolic proteins.

natural splice variant that encodes a soluble PHM protein that includes the His cluster, is stored more efficiently in regulated secretory granules than PHMcc, which lacks the His cluster (32, 52). The diminished ability of PHM/H3A to enter the regulated secretory pathway is also reflected in its increased basal secretion from PAM-1/H3A cells. As discussed below, the enhanced ability of secretagogues to stimulate secretion of the PHM/H3A that is stored in mature secretory granules reflects the inability of PAM-1/H3A to signal normally.

Very little PAM-1 is localized to the plasma membrane at steady state; antibody uptake and surface biotinylation experiments have demonstrated its rapid endocytosis, trafficking through multivesicular bodies and return to the regulated secretory pathway or degradation. Phosphorylation of multiple sites in the unstructured cytosolic domain of PAM governs the fate of internalized PAM-1 (38, 39). After endocytosis, endoproteolytic cleavage of PAM-1 at a site close to its transmembrane domain produces sPAM and an ~19-kDa C-terminal fragment. Both metabolic labeling and surface biotinylation revealed the almost total absence of sPAM/H3A in PAM-1/H3A cells. Consistent with these biochemical measurements, immunoelectron microscopy revealed diminished levels of internalized PAM-1/H3A in multivesicular bodies and their intraluminal vesicles. Lacking access to its normal endocytic trafficking pathway, internalized PAM-1/H3A is rapidly degraded. The trafficking of PAM-1 through multivesicular bodies is regulated by phosphorylation and dephosphorylation of Ser^{949} (38, 39). Our data suggest that a conformational change triggered by the His cluster when internalized PAM-1 reaches an appropriately acidified endosome plays an essential role in its endocytic trafficking.

As predicted by the lack of generation of sPAM/H3A in PAM-1/H3A cells, very little 19-kDa C-terminal fragment is created (Fig. 7*B*). γ-Secretase catalyzed intramembrane prote-

olysis of the 19- and 22/24-kDa TMD/CD fragments of PAM-1 generates sf-CD. This fragment accumulates in the nucleus in a phosphorylation state-dependent manner and is thought to play a role in controlling gene expression (16, 39). The inability of PAM-1/H3A to traverse the endocytic pathway normally largely eliminates production of sf-CD (Fig. 7, *A* and *B*).

Role of PAM His Cluster in Signaling—Using a doxycycline inducible system to control PAM-1 expression in AtT-20 cells, we demonstrated that expression of PAM-1 causes changes in gene expression, inhibits POMC processing, reduces the ability of secretagogue to stimulate secretory granule exocytosis, and alters cytoskeletal organization (16, 32). Expression of similar levels of PAM-1/H3A does not alter POMC processing, secretagogue responsiveness, or cytoskeletal organization. These differences could be a direct reflection of the altered properties of PAM-1/H3A or an indirect effect of the inability of PAM-1/H3A to traffic normally, generate sf-CD, and alter gene expression (Fig. 10*E*).

Because mutating the His cluster in the linker region of PAM-1 would be expected to result in a loss-of-function phenotype, we conclude that one of the normal roles of PAM is to serve as a pH sensor in the regulated secretory pathway and in the endocytic pathway. The inability of low luminal pH to alter the conformation of the cytosolic domain of PAM-1/H3A as it traverses specific subcellular locations could alter its ability to interact with essential cytosolic proteins like Kalirin and Uhmk1 (16). Lacking the ability to traverse the endocytic pathway, PAM-1/H3A may never be exposed to the enzymes that allow PAM-1 to undergo the sequential cleavages needed to produce sf-CD and signal from the lumen to the cytosol. Using antisera specific to Ser(P)^{937} and Thr(P)^{946}, Ser(P)^{949}, we were unable to detect changes in the steady state phosphorylation of PAM-1/H3A, but changes in phosphorylation at specific subcellular locations may occur.

Like PAM-1/H3A, PAM-1 proteins bearing cytosolic domain mutations that eliminate their ability to interact with Uhmk-1 (K919R; L926Q; F929A,F930A), a Ser/Thr protein kinase that phosphorylates Ser^{949}, lose their ability to alter regulated secretion and cytoskeletal organization (14, 55). Although PAM-1/K919R and PAM-1/F929A,F930A generate normal amounts of sf-CD, altered sf-CD phosphorylation would be expected to alter its ability to signal. Due to the presence of different interactors, a pH-dependent conformational change in the linker domain of PAM-1 that is entering immature secretory granules may trigger a different cytosolic response than a pH-dependent conformational change that occurs when PAM-1 is traversing the endocytic pathway.

Acknowledgments—We thank Darlene D'Amato and Yanping Wang for making these experiments possible, Mathilde Bonnemaison for suggestions on immunofluorescence and surface biotinylation protocols, and Dr. Mark Maciejewski for conducting trial NMR experiments. We thank the Electron Microscopy Unit of the Institute of Biotechnology, University of Helsinki, for providing laboratory facilities.

REFERENCES

1. Colomer, V., Kicska, G. A., and Rindler, M. J. (1996) Secretory granule content proteins and the luminal domains of granule membrane proteins aggregate *in vitro* at mildly acidic pH. *J. Biol. Chem.* **271,** 48–55
2. Kuliawat, R., and Arvan, P. (1992) Protein targeting via the "constitutive-like" secretory pathway in isolated pancreatic islets: passive sorting in the immature granule compartment. *J. Cell Biol.* **118,** 521–529
3. Dancourt, J., and Barlowe, C. (2010) Protein sorting receptors in the early secretory pathway. *Annu. Rev. Biochem.* **79,** 777–802
4. Appenzeller-Herzog, C., Roche, A. C., Nufer, O., and Hauri, H. P. (2004) pH-induced conversion of the transport lectin ERGIC-53 triggers glycoprotein release. *J. Biol. Chem.* **279,** 12943–12950
5. Wu, M. M., Grabe, M., Adams, S., Tsien, R. Y., Moore, H. P., and Machen, T. E. (2001) Mechanisms of pH regulation in the regulated secretory pathway. *J. Biol. Chem.* **276,** 33027–33035
6. Dickson, E. J., Duman, J. G., Moody, M. W., Chen, L., and Hille, B. (2012) Orai-STIM-mediated Ca^{2+} release from secretory granules revealed by a targeted Ca^{2+} and pH probe. *Proc. Natl. Acad. Sci. U.S.A.* **109,** E3539-E3548
7. Sobota, J. A., Ferraro, F., Bäck, N., Eipper, B. A., and Mains, R. E. (2006) Not all secretory granules are created equal: Partitioning of soluble content proteins. *Mol. Biol. Cell* **17,** 5038–5052
8. Milgram, S. L., Kho, S. T., Martin, G. V., Mains, R. E., and Eipper, B. A. (1997) Localization of integral membrane peptidylglycine α-amidating monooxygenase in neuroendocrine cells. *J. Cell Sci.* **110,** 695–706
9. Eipper, B. A., Bloomquist, B. T., Husten, E. J., Milgram, S. L., and Mains, R. E. (1993) Peptidylglycine α-amidating monooxygenase and other processing enzymes in the neurointermediate pituitary. *Ann. N.Y. Acad. Sci.* **680,** 147–160
10. Lee, S. N., Prodhomme, E., and Lindberg, I. (2004) Prohormone convertase 1 (PC1) processing and sorting: effect of PC1 propeptide and proSAAS. *J. Endocrinol.* **182,** 353–364
11. Lee, S. N., Kacprzak, M. M., Day, R., and Lindberg, I. (2007) Processing and trafficking of a prohormone convertase 2 active site mutant. *Biochem. Biophys. Res. Commun.* **355,** 825–829
12. Greene, D., Das, B., and Fricker, L. D. (1992) Regulation of carboxypeptidase E. Effect of pH, temperature and Co^{2+} on kinetic parameters of substrate hydrolysis. *Biochem. J.* **285,** 613–618
13. Fricker, L. D. (1988) Activation and membrane binding of carboxypeptidase E. *J. Cell. Biochem.* **38,** 279–289
14. Steveson, T. C., Zhao, G. C., Keutmann, H. T., Mains, R. E., and Eipper, B. A. (2001) Access of a membrane protein to secretory granules is facilitated by phosphorylation. *J. Biol. Chem.* **276,** 40326–40337
15. Rajagopal, C., Stone, K. L., Mains, R. E., and Eipper, B. A. (2010) Secretion stimulates intramembrane proteolysis of a secretory granule membrane enzyme. *J. Biol. Chem.* **285,** 34632–34642
16. Francone, V. P., Ifrim, M. F., Rajagopal, C., Leddy, C. J., Wang, Y., Carson, J. H., Mains, R. E., and Eipper, B. A. (2010) Signaling from the secretory granule to the nucleus: Uhmk1 and PAM. *Mol. Endocrinol.* **24,** 1543–1558
17. Poëa-Guyon, S., Ammar, M. R., Erard, M., Amar, M., Moreau, A. W., Fossier, P., Gleize, V., Vitale, N., and Morel, N. (2013) The V-ATPase membrane domain is a sensor of granular pH that controls the exocytotic machinery. *J. Cell Biol.* **203,** 283–298
18. Marshansky, V. (2007) The V-ATPase a2-subunit as a putative endosomal pH-sensor. *Biochem. Soc. Trans.* **35,** 1092–1099
19. Hurtado-Lorenzo, A., Skinner, M., El Annan, J., Futai, M., Sun-Wada, G. H., Bourgoin, S., Casanova, J., Wildeman, A., Bechoua, S., Ausiello, D. A., Brown, D., and Marshansky, V. (2006) V-ATPase interacts with ARNO and Arf6 in early endosomes and regulates the protein degradative pathway. *Nat. Cell Biol.* **8,** 124–136
20. Ludwig, M. G., Vanek, M., Guerini, D., Gasser, J. A., Jones, C. E., Junker, U., Hofstetter, H., Wolf, R. M., and Seuwen, K. (2003) Proton-sensing G-protein-coupled receptors. *Nature* **425,** 93–98
21. Rajan, S., Wischmeyer, E., Xin Liu, G., Preisig-Müller, R., Daut, J., Karschin, A., and Derst, C. (2000) TASK-3, a novel tandem pore domain acid-sensitive K^+ channel. An extracellular histiding as pH sensor. *J. Biol. Chem.* **275,** 16650–16657
22. Borza, D. B., and Morgan, W. T. (1998) Histidine-proline-rich glycoprotein as a plasma pH sensor. Modulation of its interaction with glycosaminoglycans by pH and metals. *J. Biol. Chem.* **273,** 5493–5499
23. Lauf, P. K., and Adragna, N. C. (1998) Functional evidence for a pH sensor

of erythrocyte K-Cl cotransport through inhibition by internal protons and diethylpyrocarbonate. *Cell Physiol. Biochem.* **8,** 46–60
24. Steidl, J. V., and Yool, A. J. (1999) Differential sensitivity of voltage-gated potassium channels Kv1.5 and Kv1.2 to acidic pH and molecular identification of pH sensor. *Mol. Pharmacol.* **55,** 812–820
25. Bayer, N., Schober, D., Prchla, E., Murphy, R. F., Blaas, D., and Fuchs, R. (1998) Effect of bafilomycin A1 and nocodazole on endocytic transport in HeLa cells: implications for viral uncoating and infection. *J. Virol.* **72,** 9645–9655
26. Da Poian, A. T., Carneiro, F. A., and Stauffer, F. (2009) Viral inactivation based on inhibition of membrane fusion: understanding the role of histidine protonation to develop new viral vaccines. *Protein Pept. Lett.* **16,** 779–785
27. Carneiro, F. A., Stauffer, F., Lima, C. S., Juliano, M. A., Juliano, L., and Da Poian, A. T. (2003) Membrane fusion induced by vesicular stomatitis virus depends on histidine protonation. *J. Biol. Chem.* **278,** 13789–13794
28. Hu, J., Fu, R., Nishimura, K., Zhang, L., Zhou, H. X., Busath, D. D., Vijayvergiya, V., and Cross, T. A. (2006) Histidines, heart of the hydrogen ion channel from influenza A virus: toward an understanding of conductance and proton selectivity. *Proc. Natl. Acad. Sci. U.S.A.* **103,** 6865–6870
29. Tan, J., Verschueren, K. H., Anand, K., Shen, J., Yang, M., Xu, Y., Rao, Z., Bigalke, J., Heisen, B., Mesters, J. R., Chen, K., Shen, X., Jiang, H., and Hilgenfeld, R. (2005) pH-dependent conformational flexibility of the SARS-CoV main proteinase (M(pro)) dimer: molecular dynamics simulations and multiple X-ray structure analyses. *J. Mol. Biol.* **354,** 25–40
30. Hanakam, F., Albrecht, R., Eckerskorn, C., Matzner, M., and Gerisch, G. (1996) Myristoylated and non-myristoylated forms of the pH sensor protein hisactophilin II: intracellular shuttling to plasma membrane and nucleus monitored in real time by a fusion with green fluorescent protein. *EMBO J.* **15,** 2935–2943
31. Attenborough, R. M., Hayward, D. C., Kitahara, M. V., Miller, D. J., and Ball, E. E. (2012) A "neural" enzyme in nonbilaterian animals and algae: preneural origins for peptidylglycine α-amidating monooxygenase. *Mol. Biol. Evol.* **29,** 3095–3109
32. Ciccotosto, G. D., Schiller, M. R., Eipper, B. A., and Mains, R. E. (1999) Induction of integral membrane PAM expression in AtT-20 cells alters the storage and trafficking of POMC and PC1. *J. Cell Biol.* **144,** 459–471
33. De, M., Ciccotosto, G. D., Mains, R. E., and Eipper, B. A. (2007) Trafficking of a secretory granule membrane protein is sensitive to copper. *J. Biol. Chem.* **282,** 23362–23371
34. De, M., Bell, J., Blackburn, N. J., Mains, R. E., and Eipper, B. A. (2006) Role for an essential tyrosine in peptide amidation. *J. Biol. Chem.* **281,** 20873–20882
35. Sobota, J. A., Bäck, N., Eipper, B. A., and Mains, R. E. (2009) Inhibitors of the V0 subunit of the vacuolar H^+-ATPase prevent segregation of lysosomal- and secretory-pathway proteins. *J. Cell Sci.* **122,** 3542–3553
36. Schnabel, E., Mains, R. E., and Farquhar, M. G. (1989) Proteolytic processing of pro-ACTH/endorphin begins in the Golgi complex of pituitary corticotropes and AtT-20 cells. *Mol. Endocrinol.* **3,** 1223–1235
37. Schoonderwoert, V. T., Holthuis, J. C., Tanaka, S., Tooze, S. A., and Martens, G. J. (2000) Inhibition of the vacuolar H^+-ATPase perturbs the transport, sorting, processing and release of regulated secretory proteins. *Eur. J. Biochem.* **267,** 5646–5654
38. Steveson, T. C., Keutmann, H. T., Mains, R. E., and Eipper, B. A. (1999) Phosphorylation of cytosolic domain Ser^{937} affects both biosynthetic and endocytic trafficking of peptidylglycine α-amidating monooxygenase. *J. Biol. Chem.* **274,** 21128–21138
39. Rajagopal, C., Stone, K. L., Francone, V. P., Mains, R. E., and Eipper, B. A. (2009) Secretory granule to the nucleus: role of a multiply phosphorylated intrinsically unstructured domain. *J. Biol. Chem.* **284,** 25723–25734
40. Yun, H. Y., Milgram, S. L., Keutmann, H. T., and Eipper, B. A. (1995) Phosphorylation of the cytosolic domain of peptidylglycine α-amidating monooxygenase. *J. Biol. Chem.* **270,** 30075–30083
41. Milgram, S. L., and Mains, R. E. (1994) Differential effects of temperature blockade on the proteolytic processing of three secretory granule-associated proteins. *J. Cell Sci.* **107,** 737–745
42. Eipper, B. A., Milgram, S. L., Husten, E. J., Yun, H. Y., and Mains, R. E. (1993) Peptidylglycine α-amidating monooxygenase: a multifunctional protein with catalytic, processing, and routing domains. *Protein Sci.* **2,** 489–497
43. Yun, H. Y., Keutmann, H. T., and Eipper, B. A. (1994) Alternative splicing governs sulfation of tyrosine or oligosaccharide on peptidylglycine α-amidating monooxygenase. *J. Biol. Chem.* **269,** 10946–10955
44. Tausk, F. A., Milgram, S. L., Mains, R. E., and Eipper, B. A. (1992) Expression of a peptide processing enzyme in cultured cells: truncation mutants reveal a routing domain. *Mol. Endocrinol.* **6,** 2185–2196
45. Husten, E. J., and Eipper, B. A. (1994) Purification and characterization of PAM-1, an integral membrane protein involved in peptide processing. *Arch. Biochem. Biophys.* **312,** 487–492
46. Husten, E. J., Tausk, F. A., Keutmann, H. T., and Eipper, B. A. (1993) Use of endoproteases to identify catalytic domains, linker regions, and functional interactions in soluble peptidylglycine α-amidating monooxygenase. *J. Biol. Chem.* **268,** 9709–9717
47. Milgram, S. L., Johnson, R. C., and Mains, R. E. (1992) Expression of individual forms of peptidylglycine alpha-amidating monooxygenase in AtT-20 cells: endoproteolytic processing and routing to secretory granules. *J. Cell Biol.* **117,** 717–728
48. Eipper, B. A., Green, C. B., Campbell, T. A., Stoffers, D. A., Keutmann, H. T., Mains, R. E., and Ouafik, L. (1992) Alternative splicing and endoproteolytic processing generate tissue-specific forms of pituitary peptidylglycine α-amidating monooxygenase (PAM) *J. Biol. Chem.* **267,** 4008–4015
49. Pérez-Sayáns, M., Suárez-Peñaranda, J. M., Barros-Angueira, F., Diz, P. G., Gándara-Rey, J. M., and García-García, A. (2012) An update in the structure, function, and regulation of V-ATPases: the role of the C subunit. *Braz. J. Biol.* **72,** 189–198
50. Mains, R. E., Bloomquist, B. T., and Eipper, B. A. (1991) Manipulation of neuropeptide biosynthesis through the expression of antisense RNA for peptidylglycine alpha-amidating monooxygenase. *Mol. Endocrinol.* **5,** 187–193
51. Bäck, N., Rajagopal, C., Mains, R. E., and Eipper, B. A. (2010) Secretory granule membrane protein recycles through multivesicular bodies. *Traffic* **11,** 972–986
52. Milgram, S. L., Eipper, B. A., and Mains, R. E. (1994) Differential trafficking of soluble and integral membrane secretory granule-associated proteins. *J. Cell Biol.* **124,** 33–41
53. Ferraro, F., Eipper, B. A., and Mains, R. E. (2005) Retrieval and reuse of pituitary secretory granule proteins. *J. Biol. Chem.* **280,** 25424–25435
54. Milgram, S. L., Mains, R. E., and Eipper, B. A. (1993) COOH-terminal signals mediate the trafficking of a peptide processing enzyme in endocrine cells. *J. Cell Biol.* **121,** 23–36
55. Alam, M. R., Caldwell, B. D., Johnson, R. C., Darlington, D. N., Mains, R. E., and Eipper, B. A. (1996) Novel proteins that interact with the COOH-terminal cytosolic routing determinants of an integral membrane peptide-processing enzyme. *J. Biol. Chem.* **271,** 28636–28640
56. Alam, M. R., Steveson, T. C., Johnson, R. C., Bäck, N., Abraham, B., Mains, R. E., and Eipper, B. A. (2001) Signaling mediated by the cytosolic domain of peptidylglycine α-amidating monooxygenase. *Mol. Biol. Cell* **12,** 629–644
57. Nakamura, N., Rabouille, C., Watson, R., Nilsson, T., Hui, N., Slusarewicz, P., Kreis, T. E., and Warren, G. (1995) Characterization of a cis-Golgi matrix protein, *GM130. J. Cell Biol.* **131,** 1715–1726
58. Jenks, B. G., Ederveen, A. G., Feyen, J. H., and van Overbeeke, A. P. (1985) The functional significance of glycosylation of pro-opiomelanocortin in melanotrophs of the mouse pituitary gland. *J. Endocrinol.* **107,** 365–374
59. Dröse, S., and Altendorf, K. (1997) Bafilomycins and concanamycins as inhibitors of V-ATPases and P-ATPases. *J. Exp. Biol.* **200,** 1–8
60. Zachos, C., Blanz, J., Saftig, P., and Schwake, M. (2012) A critical histidine residue within LIMP-2 mediates pH sensitive binding to its ligand β-glucocerebrosidase. *Traffic* **13,** 1113–1123
61. Williamson, D. M., Elferich, J., Ramakrishnan, P., Thomas, G., and Shinde, U. (2013) The mechanism by which a propeptide-encoded pH sensor regulates spatiotemporal activation of furin. *J. Biol. Chem.* **288,** 19154–19165
62. Qin, Z. L., Zheng, Y., and Kielian, M. (2009) Role of conserved histidine residues in the low-pH dependence of the Semliki Forest virus fusion protein. *J. Virol.* **83,** 4670–4677

63. Bell-Parikh, L. C., Eipper, B. A., and Mains, R. E. (2001) Response of an integral granule membrane protein to changes in pH. *J. Biol. Chem.* **276,** 29854–29863
64. El Kadi, N., Taulier, N., Le Huérou, J. Y., Gindre, M., Urbach, W., Nwigwe, I., Kahn, P. C., and Waks, M. (2006) Unfolding and refolding of bovine serum albumin at acid pH: ultrasound and structural studies. *Biophys. J.* **91,** 3397–3404
65. Chanat, E., and Huttner, W. B. (1991) Milieu-induced, selective aggregation of regulated secretory proteins in the trans-Golgi network. *J. Cell Biol.* **115,** 1505–1519
66. Seidah, N. G., and Prat, A. (2002) Precursor convertases in the secretory pathway, cytosol and extracellular milieu. *Essays Biochem.* **38,** 79–94
67. Ahras, M., Otto, G. P., and Tooze, S. A. (2006) Synaptotagmin IV is necessary for the maturation of secretory granules in PC12 cells. *J. Cell Biol.* **173,** 241–251